

# Driven Bose-Hubbard dimer under nonlocal dissipation: A bistable time crystal

C. Lledó,<sup>1,\*</sup> Th. K. Mavrogordatos,<sup>2</sup> and M. H. Szymańska<sup>1</sup>

<sup>1</sup>*Department of Physics and Astronomy, University College London,  
Gower Street, London, WC1E 6BT, United Kingdom*

<sup>2</sup>*Department of Physics, Stockholm University, SE-106 91, Stockholm, Sweden*

(Dated: August 14, 2019)

We investigate the critical behavior of the open coherently-driven Bose-Hubbard dimer under non-local dissipation. A conserved quantity arises from the nonlocal nature of the dissipation, rendering the dimer multistable. In the weak-coupling semiclassical limit, the displayed criticality takes the form of amplitude bistability and breaking of spatial and temporal symmetries. A period-bistable time crystal is formed, consisting of Josephson-like oscillations. Mean-field dynamics and quantum trajectories complement the spectral analysis of the Liouvillian in the approach to the semiclassical limit.

PACS numbers: 05.30.Jp, 42.50.Pq, 42.65.Pc

Keywords: Bose-Hubbard dimer, dissipative quantum phase transitions, nonlocal dissipation, multistability

## I. INTRODUCTION

Phase transitions substantiated by a mean-field bifurcation have been intimately tied to the evolution of quantum optics. Characteristic cases include the Dicke phase transition [1], co-operative resonance fluorescence [2], and the laser [3]. The study of quantum phase transitions in zero dimensions [4] far from thermal equilibrium reappraises the definition of the thermodynamic limit alongside the distinct role of quantum fluctuations, taking the form of an ostensible deviation from the mean-field dynamics [5, 6]. Furthermore, the work of Ref. [7] has already drawn the analogy between quantum phase transitions in closed systems and dissipative phase transitions (DPTs) in open quantum systems, through analyzing the spectrum of the Liouvillian, while the properties of the steady state have been assessed with respect to the particular critical eigenvalue defining the Liouvillian spectral gap [8]. To date, DPTs attract a significant and ongoing interest among the communities of cold atoms, circuit QED, and semiconductors (see, e.g., Refs. [9–16]).

In that background, the interplay between coherence and dissipation renders the Bose-Hubbard dimer (BHD) a suitable candidate for assessing the role of conserved quantities and the associated symmetries in dissipative quantum phase transitions. A transition from intermittent entanglement to a persistently entangled state was demonstrated a few years ago for a dissipative BHD [17]. The standard phenomenological approach to dissipation amounts typically to the definition of a Liouville super-operator governing the system response, assessed against its coherent evolution. Statistical independence of the reservoirs the system is coupled to gives rise to the configuration of *local dissipation*, while coupling to one common bosonic reservoir generates *nonlocal dissipation*.

Critical behavior in the presence of a coherent drive, leading to symmetry breaking, has been very recently

taken up for local dissipation when characterizing the quantum correlation properties of the BHD [18, 19]. In many cases, local dissipation is well justified and often greatly simplifies the analysis of the transient and the steady state. In reality, however, different collective modes have different dissipation rates, giving rise to some amount of nonlocal dissipation.

In this work, we demonstrate the importance of the nonlocality of the dissipation in the open coherently-driven BHD. A continuous swapping symmetry together with a conserved quantity arises, leading to the occurrence of quantum multistability [20]. Alongside the familiar first-order DPT [21] associated with semiclassical amplitude bistability, with origins in the quantum Duffing oscillator [22], the BHD breaks the spatial swapping symmetry as well as the time invariance of the steady state. By studying the closure of the Liouvillian gap as we approach a weak-coupling semiclassical limit, we show that a dissipative time-crystal [23–29] with Josephson-like oscillations is formed. We find that two different time-crystalline periods coexist in the parameter regime of semiclassical bistability. We employ and compare the semiclassical Gross-Pitaevskii equations, quantum trajectories, and numerical solutions of the Master Equation in a truncated Hilbert space in order to fully appreciate the novel phases.

## II. THE MODEL

We consider a BHD whose dynamical evolution is governed by the Lindblad equation (with  $\hbar = 1$ )

$$\partial_t \hat{\rho} = -i[\hat{\mathcal{H}}, \hat{\rho}] + \gamma \mathcal{D}[\hat{a}_1 + \hat{a}_2](\hat{\rho}) \equiv \mathcal{L}(\hat{\rho}). \quad (1)$$

Here,  $\mathcal{D}[\hat{L}](\bullet) = \hat{L} \bullet \hat{L}^\dagger - (1/2)\{\hat{L}^\dagger \hat{L}, \bullet\}$  is the dissipator, while the system Hamiltonian under coherent drive, in a

\* electronic address: c.lledo.17@ucl.ac.uk

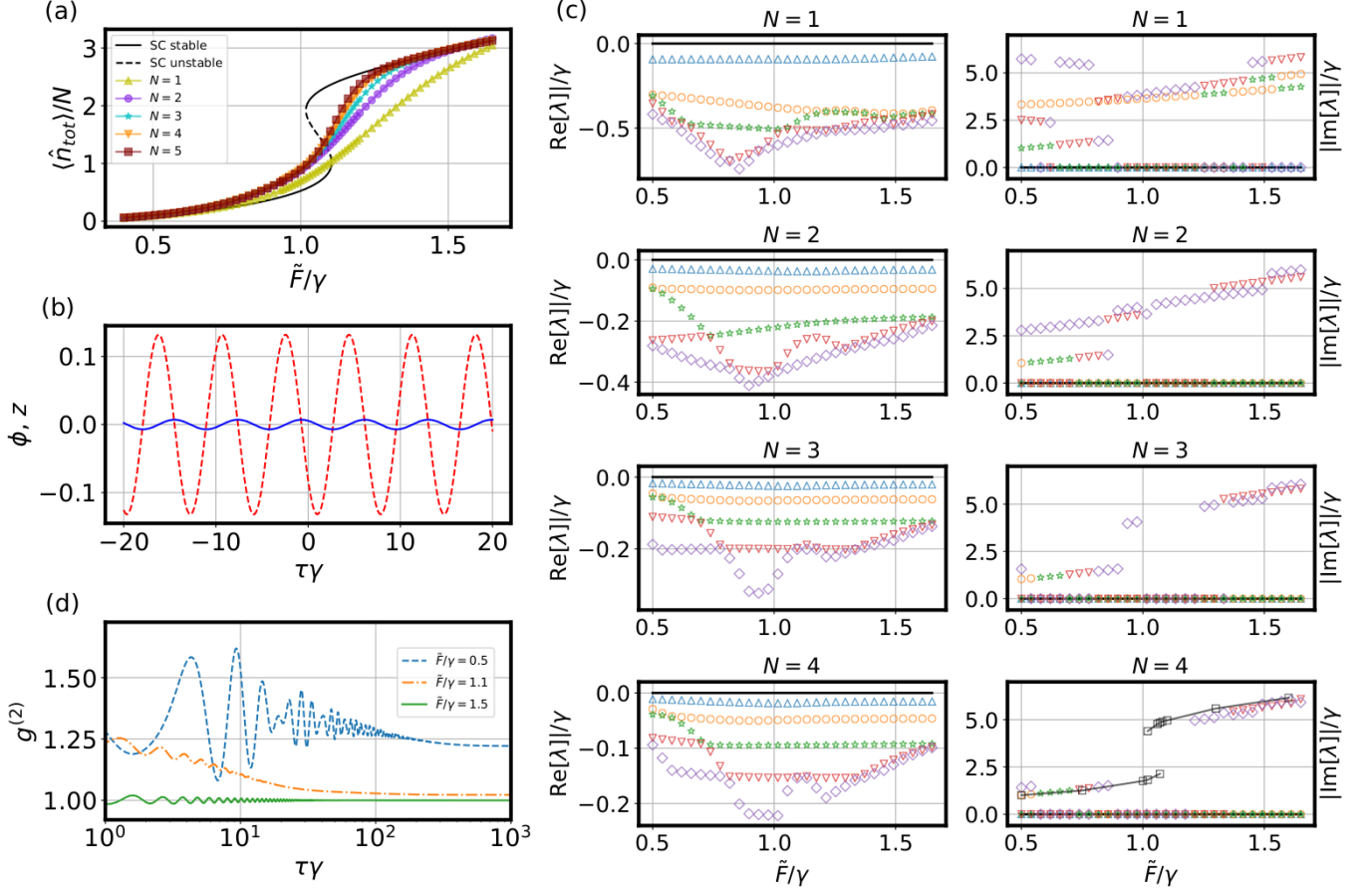


FIG. 1. Limit cycles and the Liouvillian spectrum. (a), (c) Steady-state total number of bosons  $\langle \hat{n}_{\text{tot}} \rangle / N$  and the first five Liouvillian gaps, respectively, as a function of  $\tilde{F}/\gamma$  for different values of  $N$ . In (a) the black solid and dashed lines, denoted by  $SC$ , depict semiclassical predictions. In (c) the semiclassical limit-cycle frequencies are juxtaposed (in black squares) to the plot depicting the imaginary part of the gaps for  $N = 4$ . (b) Relative phase  $\phi = \text{Arg}[\alpha_1] - \text{Arg}[\alpha_2]$  (dashed red) and population difference  $z = (|\alpha_1|^2 - |\alpha_2|^2)/N$  (blue) versus time in the semiclassical Josephson limit cycle for  $\tilde{F}/\gamma = 0.4$ . The  $40\gamma^{-1}$  time window is centered around  $t_0 = 3.5 \times 10^5 \gamma^{-1}$ . (d) Quantum second-order correlation function  $g^{(2)}(\tau)$  (symmetric with respect to the two modes  $i = 1, 2$ ) for three different pump amplitudes in the quantum regime and  $N = 5$ . The parameters are:  $\Delta/\gamma = 0.7$ ,  $J/\gamma = 1.5$ , and  $\tilde{U}/\gamma = 1$ . The Fock space per site is truncated at 10, 14, 18, 21, and 24 bosons for  $N = 1, 2, 3, 4$ , and 5, respectively.

frame rotating with the pump frequency  $\omega_p$ , reads

$$\hat{\mathcal{H}} = \sum_{i=1,2} -\Delta \hat{a}_i^\dagger \hat{a}_i + U \hat{a}_i^\dagger \hat{a}_i^\dagger \hat{a}_i \hat{a}_i + F(\hat{a}_i^\dagger + \hat{a}_i) - J(\hat{a}_1^\dagger \hat{a}_2 + \hat{a}_1 \hat{a}_2^\dagger), \quad (2)$$

where  $\hat{a}_i$  is the  $i$ -mode bosonic annihilation operator,  $\Delta = \omega_p - \omega_c$  is the detuning between the pump and the resonant mode frequencies,  $\omega_p$  and  $\omega_c$  respectively,  $U$  is the interaction strength,  $F$  is the driving amplitude, and  $J$  is the intermode coupling. For nonlocal dissipation,  $\hat{L} = \hat{a}_1 + \hat{a}_2$ . The driving term originates from the interaction of the two bosonic modes  $\hat{a}_{1,2}$  with a coherent source treated as a (semi)classical field. Drive and decay only affect the bonding mode  $(\hat{a}_1 + \hat{a}_2)/\sqrt{2}$ , which couples to the antibonding mode  $(\hat{a}_1 - \hat{a}_2)/\sqrt{2}$  solely via the nonlinearity. We rescale the pump amplitude and

the interaction with the help of a generic parameter  $N$  (the analog of the laser saturation photon number, for instance), as  $F = \sqrt{N}\tilde{F}$  and  $U = \tilde{U}/N$ , such that  $\sqrt{U}F$  is constant for any  $N$ . This allows us to consider a well defined weak-coupling thermodynamic limit,  $N \rightarrow \infty$ , where the boson number diverges ( $\langle \hat{a}_i^\dagger \hat{a}_i \rangle \propto N$ ). In this limit, quantum fluctuations are negligible, and a semiclassical analysis is adequate [19]. Our system exhibits *three* important properties delineated below.

*The first one* is the presence of a continuous symmetry  $\mathcal{L}(\hat{U}(\phi) \bullet \hat{U}(\phi)^\dagger) = \hat{U}(\phi) \mathcal{L}(\bullet) \hat{U}(\phi)^\dagger$  generated by the unitary operator  $\hat{U}(\phi) = e^{i\phi \hat{Z}_2}$  (for real  $\phi$ ), with the swapping operator  $\hat{Z}_2 = \sum_{n_1, n_2} |n_1, n_2\rangle \langle n_2, n_1|$  (written in the Fock-state basis of the two individual modes). The swapping operator is a conserved quantity. This is only possible due to the nonlocality of the dissipation [30] and

is the origin of *quantum multistability* [20]. Since there are infinitely-many possible initial expectation values of  $\hat{Z}_2$ , there are also infinitely-many steady states. This is true for any value of  $N$ . For a finite  $N$ , the steady state reads  $\hat{\rho}_{\text{ss}} = \hat{r}_{0,1} + c_{0,2}\hat{r}_{0,2}$ , where  $\hat{r}_{0,1}$  is a density matrix while  $\hat{r}_{0,2}$  is not, and the coefficient  $c_{0,2} = \text{Tr}[\hat{Z}_2\hat{\rho}(0)]$  depends on the initial condition. This steady state is symmetric, i.e.,  $\hat{U}(\phi)\hat{\rho}_{\text{ss}}\hat{U}^\dagger(\phi) = \hat{\rho}_{\text{ss}}$ , irrespective of the initial condition.

*Secondly*, the system we consider presents limit cycles [31] in the limit  $N \rightarrow \infty$ . These are persistent periodic oscillations in the infinite time limit of the dynamical evolution. Recently, an open quantum system with this property has been termed a *boundary time crystal* [24]. It is there argued that while the total Hamiltonian (of the boundary, the bulk, and their coupling interaction) is time-translation invariant, the boundary system presents limit cycles, thus breaking the global time-translation symmetry and forming *time crystal* with a nonrigid period that is allowed to change continuously as a function of the system parameters. Our system satisfies the same conditions. The dependence on the period of the coherent drive can be eliminated by a gauge transformation. This means that any emergent periodic response stems from a continuous breaking of time-translation invariance in contrast to the discrete fashion due to the presence of a Floquet-map eigenvalue in the unit circle [25, 28]. The steady state of the BHD, which spontaneously breaks the time-translation invariance of the Liouvillian, assumes the form (for  $N \rightarrow \infty$ )

$$\hat{\rho}_{\text{ss}}(t) = \hat{r}_{0,1} + \sum_{d=2}^{D_0} c_{0,d} \hat{r}_{0,d} + \sum_{d=1}^{D_1} (c_{1,d} e^{i|\lambda_1|t} \hat{r}_{1,d} + \text{H.c.}), \quad (3)$$

where  $\mathcal{L}(\hat{r}_{n,d}) = \lambda_n \hat{r}_{n,d}$ ,  $c_{n,d}$  are coefficients depending on the initial system density matrix  $\hat{\rho}(0)$ , and  $\lambda_1$  is a purely imaginary eigenvalue responsible for the formation of a limit cycle [32]. The upper limits  $D_0$  and  $D_1$  in the sums of the right-hand side in Eq. (3) are unknown. The index  $d = 1, \dots, D_n$  labels the degeneracy of the eigenvalue  $\lambda_n$ . In principle, one could prepare an initial condition such that the coefficients  $c_{1,d}$  vanish and the system reaches a time-independent steady state. For a system prepared in such a manner, an infinitesimal disturbance would lead to  $c_{1,d} \neq 0$  with some degeneracy  $d$ , causing the response to oscillate ceaselessly and forming a time crystal. This could in principle be observed in any time-delayed two-point measurement.

*Finally*, the system response is determined by semiclassical complex-amplitude bistability as  $N \rightarrow \infty$ . This is known to occur in the BHD under local dissipation for the same driving configuration as the one we consider here [33]. Semiclassical bistability manifests itself as a region in the parameter space where two semiclassical fixed points, with different complex amplitudes, appear. In our model, we will show that two attractors, specifically limit cycles with different periods, coexist in this region.

### III. RESULTS

In order to assess the system behavior as  $N \rightarrow \infty$  we resort to the Gross-Pitaevskii (semiclassical) approach, in which the operators in the Heisenberg picture are replaced by their expectation values  $\alpha_i = \langle \hat{a}_i \rangle$ . We remark that our continuous swapping symmetry is intrinsically quantum and cannot be captured by the semiclassical picture, where it shows up merely as a discrete swapping symmetry  $\alpha_1 \leftrightarrow \alpha_2$ . We compare the semiclassical predictions with the calculations in the quantum regime for increasing values of  $N$ .

In Fig. 1(a) we depict the steady state expectation value of the rescaled total number of bosons  $\hat{n}_{\text{tot}}/N = (\hat{a}_1^\dagger \hat{a}_1 + \hat{a}_2^\dagger \hat{a}_2)/N$  as a function of the rescaled pump amplitude  $\bar{F}/\gamma = F/(\sqrt{N}\gamma)$ . We present in color the quantum results for different values of  $N$ . The continuous (dashed) black lines indicate stable (unstable) semiclassical fixed points. One can see that as  $N$  increases, the occupation number in the quantum regime approaches one of the two semiclassical stable branches. The transition between the two branches becomes increasingly sharper, suggesting the formation of a discontinuous jump, as one would expect from a first-order DPT [8, 21].

The basin of attraction of the stable fixed points is just the two-dimensional plane given by  $\alpha_1 = \alpha_2$  in the four-dimensional phase space defined by the real and imaginary parts of  $\alpha_1$  and  $\alpha_2$ . A randomly chosen initial condition generates a trajectory that most certainly avoids the plane, converging to one of the families of limit cycles which revolve around the stable fixed points. The amplitude of the attained limit cycle is determined by the initial difference in the coherent states  $\alpha_1(0) - \alpha_2(0)$ , although its period is solely dependent on the set of parameters entering in Eq. (1), except in the region of bistability, where limit cycles with two different frequencies have different basins of attraction. Interestingly, the limit cycles break the swapping symmetry. They are the so-called *Josephson oscillations*. A typical example of these oscillations is depicted in Fig. 1(b).

In Fig. 1(d), we show the five eigenvalues whose real parts are closer to zero (defining the sequence of the gaps), for increasing values of  $N$ . We distinguish them using different colors and markers according to the proximity of their real parts to the zero eigenvalue (which is doubly degenerate—for the identity and the swapping operator). We consider only one of the two complex eigenvalues forming a conjugate pair. It is evident that all the gaps are closing with growing  $N$ . Eigenvalue crossings are also visible, while for moderate pump strengths there is an eigenvalue with an *inverted-parabolic shape*, flattening to zero as  $N$  increases. This eigenvalue has zero imaginary part, suggesting that it is itself responsible for a first-order DPT in the thermodynamic limit mediated by the presence of bistability [8].

In addition, there are two eigenvalues with a nonzero imaginary part at low and high pump strengths. Their imaginary parts converge very quickly for relatively small

$N$  (at  $\tilde{F}/\gamma = 1.65$  we have a maximum of  $\sim 13$  bosons for  $N = 4$ ). These are the eigenvalues responsible for the limit cycles as  $N \rightarrow \infty$ . To illustrate this point, we show the frequencies of the semiclassical limit cycles (in black squares) in the plot  $N = 4$ . For low pump values, the scaled frequency  $\text{Im}[\lambda]/\gamma$  has already reached its  $N \rightarrow \infty$  value for  $N = 4$ . As we have already anticipated, two limit cycles with different periods coexist in the semiclassical bistable region ( $1.02 \lesssim \tilde{F}/\gamma \lesssim 1.1$ ). Either one or the other is reached in the long-time limit, depending on the amplitude of the initial coherent state.

The closure of the first gap for all the pump values we have considered suggests a critical slowing down transcending the bistability region, in contrast with local dissipation [32]. To show this we employ the time-delayed second-order correlation function [16] (symmetric with respect to the two modes  $i = 1, 2$ )  $g^{(2)}(\tau) = \langle \hat{a}_i^\dagger(0)\hat{a}_i^\dagger(\tau)\hat{a}_i(\tau)\hat{a}_i(0) \rangle_{\text{ss}} / \langle \hat{a}_i^\dagger\hat{a}_i \rangle_{\text{ss}}^2 = \text{Tr}[\hat{a}_i^\dagger(0)\hat{a}_i(0)e^{\tau\mathcal{L}(\hat{\rho}')} / \langle \hat{a}_i^\dagger\hat{a}_i \rangle_{\text{ss}}$ , where  $\hat{\rho}' = \hat{a}_i\hat{\rho}_{\text{ss}}\hat{a}_i^\dagger / \text{Tr}[\hat{a}_i\hat{\rho}_{\text{ss}}\hat{a}_i^\dagger]$  is the state of the system after an initial detection of the mode  $i$  and is evolved during a time  $\tau$  before making a second measurement. The subscript ss refers to the steady state. After a sufficiently long time, if the steady state is unique,  $g^{(2)}(\tau)$  will relax to the value of 1, due to its normalization. In Fig. 1(c) we plot  $g^{(2)}(\tau)$  for three pump values. One can observe that the correlations take a long time to decay for  $\tilde{F}/\gamma = 0.5$ , far below the bistability region. Furthermore, the function does not always converge to 1. This is a clear manifestation of the infinite number of steady states: The initial detection changes the value of the conserved quantity  $\langle \hat{Z}_2 \rangle$ , so the system must relax to a different steady state.

Figure 2 clearly depicts the emergence of the periodic oscillations as  $N \rightarrow \infty$ . In frames (b) and (c), we can observe frequency bistability, starting from two different initial conditions. Here we are in the semiclassical bistability region with finite  $N$ , where the oscillations are damped. Moreover, we show in Ref. [32] that single trajectories Fourier transform as well to a neat frequency peak matching that of the semiclassical response (apart from a small deviation due to stochastic jumps).

In the bistability region, a single quantum trajectory evidences switching between the dim and bright metastable states [6]. This is accompanied by a frequency switch for the oscillations between the two (frequency) branches drawn in Fig. 1(c) for  $N = 4$ . However, for large but finite  $N$ , the inverse of the switching rate is larger than the lifetime of the oscillations, which means that on average one obtains an oscillation frequency corresponding to either the lower or the upper branches of Fig. 1(c), depending on the initial condition [see Figs. 2(b) and 2(c)].

In Fig. 2(c), one can notice a mismatch between the frequency peaks in the semiclassical and the quantum regimes for  $N = 25$ . There are two reasons for this: (i) the semiclassical evolution remains transient and the fre-

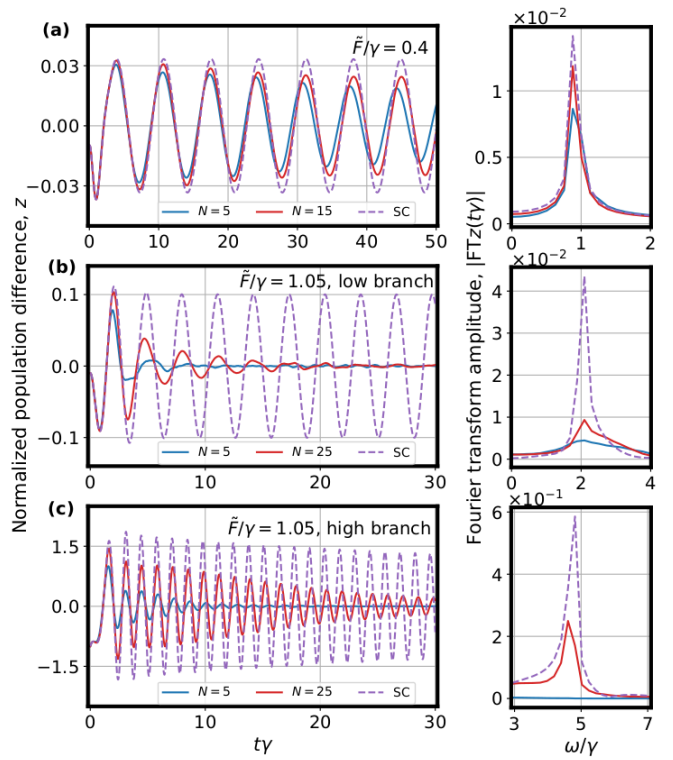


FIG. 2. Emergence of limit-cycle oscillations. Normalized population difference  $z = \langle \hat{a}_1^\dagger\hat{a}_1 - \hat{a}_2^\dagger\hat{a}_2 \rangle / N$  as a function of time and the respective Fourier transform for two different pump values:  $\tilde{F}/\gamma = 0.4$  in (a) and  $\tilde{F}/\gamma = 1.05$  in (b) and (c). The initial condition is a scaled coherent state  $|\alpha_1 = 0, \alpha_2 = 0.1\sqrt{N}\rangle$  in (a) and (b) and  $|\alpha_1 = 0, \alpha_2 = \sqrt{N}\rangle$  in (c). In the bistability region ( $\tilde{F}/\gamma = 1.05$ ) these initial states lead to the lower and upper semiclassical branches [see Fig. 1(a)], respectively. For finite  $N$ , the results in (a) are obtained by solving Eq. (1), while in (b) and (c) by averaging over 5000 quantum trajectories. The Fock space per site is truncated at 30 bosons for  $N = 15$  in (a) and at 90 for  $N = 25$  in (b) and (c). The rest of the parameters are the same as in Fig. 1.

quency has not yet attained its limit-cycle value (which depends nonlinearly on the mode population and therefore decreases in the long-time limit), (ii) the imaginary part of the Liouvillian eigenvalue responsible for the oscillations has not yet converged to its  $N \rightarrow \infty$  value.

We now propose a mechanism accounting for the observed periodic oscillations. When  $\tilde{U} = 0$ , bonding and antibonding modes are decoupled, and the antibonding mode evolves coherently giving trivial periodic oscillations in both the quantum and semiclassical regimes. When  $\tilde{U} \neq 0$ , the interaction term becomes very inefficient in coupling both modes when the antibonding-mode population is sufficiently small. The emergence of the limit cycles is then due to an effective decoupling between the two modes (see also Ref. [32] for further details).

#### IV. DISCUSSION

Nonlocal dissipation for open quantum systems without detailed balance has been considered in the context of noiseless subsystems or decoherence-free subspaces [34, 35], in cold atoms or many-body spin systems [24, 36–38], and in a recent proposal of a Floquet time crystal [25]. In general, that type of dissipation is either engineered or appears as a consequence of photon-mediated long range interactions. The specific form of Eq. (1) can be derived [32] from first principles if one considers that both modes in our system have the exact same coupling with a single bosonic bath. This approach is similar to Ref. [34].

In practice, the assumption of identical coupling between the two modes and the environment is idealistic. While the coupling strength between the two system modes and the reservoir modes (with frequencies in the vicinity of the driving frequency) could be equal, in general the relative phases will be different [32]. This implies a mixture of bonding and antibonding dissipation and, in turn, the mixture of local and nonlocal dissipation following a change of basis. An important question, then, concerns the implications of a broken symmetry with respect to the swapping operation in the presence of a small yet non-negligible amount of dissipation for the antibonding mode. This perturbation has the consequence of lifting the degeneracy of the zero eigenvalue in the Liouvillian spectrum and also destroying the limit cycles. However, as we show in Ref. [32], periodic os-

cillations persist for long times, and the time-crystalline period is robust.

The BHD has already been studied in the laboratory [14]. The type of dissipation in our model could be realized in a circuit QED experiment coupling two degenerate modes to a microwave resonator at a single spatial location, where the wave function overlap between the resonator mode and both system modes is identical. Alternatively, it could be realized with polaritons in two coupled semiconductor micropillars if the bonding and antibonding mode linewidths differ by two orders of magnitude or more. This could be achieved by etching the sample in such a way that the nonradiative losses [39] of the bonding mode make the dominant part of the total dissipation.

#### ACKNOWLEDGMENTS

We are thankful to the developers of the Quantum Toolbox in Python (QuTiP) [40, 41], as we have used it for most of our calculations in the quantum regime. We thank A. Amo, E. Ginossar, and M. Stern for helpful discussions, and J. Keeling for the careful reading of the manuscript. C.L. gratefully acknowledges the financial support of CONICYT through Becas Chile 2017, Contract No. 72180352. M.H.S. gratefully acknowledges financial support from QuantERA InterPol and EPSRC (Grant No. EP/R04399X/1 and No. EP/K003623/2).

- 
- [1] P. Kirton, M. M. Roses, J. Keeling, and E. G. Dalla Torre, *Adv. Quantum Technol.* **2**, 1970013 (2019).
  - [2] L. M. Narducci, D. H. Feng, R. Gilmore, and G. S. Agarwal, *Phys. Rev. A* **18**, 1571 (1978).
  - [3] V. DeGiorgio and M. O. Scully, *Phys. Rev. A* **2**, 1170 (1970).
  - [4] M.-J. Hwang, R. Puebla, and M. B. Plenio, *Phys. Rev. Lett.* **115**, 180404 (2015).
  - [5] C. M. Savage and H. J. Carmichael, *IEEE Journal of Quantum Electronics* **24**, 1495 (1988).
  - [6] H. J. Carmichael, *Phys. Rev. X* **5**, 031028 (2015).
  - [7] E. M. Kessler, G. Giedke, A. Imamoglu, S. F. Yelin, M. D. Lukin, and J. I. Cirac, *Phys. Rev. A* **86**, 012116 (2012).
  - [8] F. Minganti, A. Biella, N. Bartolo, and C. Ciuti, *Phys. Rev. A* **98**, 042118 (2018).
  - [9] F. Dimer, B. Estienne, A. S. Parkins, and H. J. Carmichael, *Phys. Rev. A* **75**, 013804 (2007).
  - [10] K. Baumann, C. Guerlin, F. Brennecke, and T. Esslinger, *Nature (London)* **464**, 1301 (2010), 0912.3261.
  - [11] K. Baumann, R. Mottl, F. Brennecke, and T. Esslinger, *Phys. Rev. Lett.* **107**, 140402 (2011).
  - [12] F. Brennecke, R. Mottl, K. Baumann, R. Landig, T. Donner, and T. Esslinger, *PNAS* **110**, 11763 (2013).
  - [13] M. Fitzpatrick, N. M. Sundaresan, A. C. Y. Li, J. Koch, and A. A. Houck, *Phys. Rev. X* **7**, 011016 (2017).
  - [14] S. R. K. Rodriguez, W. Casteels, F. Storme, N. Carlon Zambon, I. Sagnes, L. Le Gratiet, E. Galopin, A. Lemaître, A. Amo, C. Ciuti, and J. Bloch, *Phys. Rev. Lett.* **118**, 247402 (2017).
  - [15] J. M. Fink, A. Dombi, A. Vukics, A. Wallraff, and P. Domokos, *Phys. Rev. X* **7**, 011012 (2017).
  - [16] T. Fink, A. Schade, S. Höfling, C. Schneider, and A. Imamoglu, *Nat. Phys.* **14**, 365 (2018).
  - [17] T. Pudlik, H. Hennig, D. Witthaut, and D. K. Campbell, *Phys. Rev. A* **88**, 063606 (2013).
  - [18] B. Cao, K. W. Mahmud, and M. Hafezi, *Phys. Rev. A* **94**, 063805 (2016).
  - [19] W. Casteels and C. Ciuti, *Phys. Rev. A* **95**, 013812 (2017).
  - [20] V. V. Albert and L. Jiang, *Phys. Rev. A* **89**, 022118 (2014).
  - [21] W. Casteels, R. Fazio, and C. Ciuti, *Phys. Rev. A* **95**, 012128 (2017).
  - [22] P. D. Drummond and D. F. Walls, *J. Phys. A: Math. Gen.* **13**, 725 (1980).
  - [23] K. Sacha and J. Zakrzewski, *Rep. Prog. Phys.* **81**, 016401 (2018).
  - [24] F. Iemini, A. Russomanno, J. Keeling, M. Schirò, M. Dalmonte, and R. Fazio, *Phys. Rev. Lett.* **121**, 035301 (2018).
  - [25] R. R. W. Wang, B. Xing, G. G. Carlo, and D. Poletti,

- Phys. Rev. E **97**, 020202(R) (2018).
- [26] J. O’Sullivan, O. Lunt, C. W. Zollitsch, M. Thewalt, J. J. Morton, and A. Pal, arXiv:1807.09884 (2018).
- [27] K. Tucker, B. Zhu, R. Lewis-Swan, J. Marino, F. Jimenez, J. Restrepo, and A. M. Rey, New J. Phys. **20**, 123003 (2018).
- [28] Z. Gong, R. Hamazaki, and M. Ueda, Phys. Rev. Lett. **120**, 040404 (2018).
- [29] F. M. Gambetta, F. Carollo, M. Marcuzzi, J. P. Garrahan, and I. Lesanovsky, Phys. Rev. Lett. **122**, 015701 (2019).
- [30] D. Nigro, J. Stat. Mech. **2019**, 043202 (2019).
- [31] Note that the limit cycles are not a consequence of having a nontrivial conserved operator ( $\hat{Z}_2$ ). The same BHD model, but with antisymmetric drive, also exhibits limit cycles and only  $\hat{1}$  is conserved.
- [32] See the Supplemental Material for further details, which includes Refs. [42–50].
- [33] W. Casteels and M. Wouters, Phys. Rev. A **95**, 043833 (2017).
- [34] P. Zanardi and M. Rasetti, Phys. Rev. Lett. **79**, 3306 (1997); P. Zanardi, Phys. Rev. A **57**, 3276 (1998).
- [35] D. A. Lidar, I. L. Chuang, and K. B. Whaley, Phys. Rev. Lett. **81**, 2594 (1998).
- [36] D. F. V. James, Phys. Rev. A **47**, 1336 (1993).
- [37] B. Olmos, D. Yu, and I. Lesanovsky, Phys. Rev. A **89**, 023616 (2014).
- [38] C. D. Parmee and N. R. Cooper, Phys. Rev. A **97**, 053616 (2018).
- [39] N. C. Zambon, P. St-Jean, M. Milićević, A. Lemaitre, A. Harouri, L. LeGratiet, O. Bleu, D. Solnyshkov, G. Malpuech, I. Sagnes, S. Ravets, A. Amo, and J. Bloch, Nat. Photonics **13**, 283 (2019).
- [40] J. Johansson, P. Nation, and F. Nori, Comput. Phys. Commun. **183**, 1760 (2012).
- [41] J. Johansson, P. Nation, and F. Nori, Comput. Phys. Commun. **184**, 1234 (2013).
- [42] B. Buca, J. Tindall, and D. Jaksch, Nat. Commun. **10** (2019).
- [43] I. L. Aleiner, B. L. Altshuler, and Y. G. Rubo, Phys. Rev. B **85**, 121301(R) (2012).
- [44] K. Rayanov, B. L. Altshuler, Y. G. Rubo, and S. Flach, Phys. Rev. Lett. **114**, 193901 (2015).
- [45] K. Macieszczak, M. Guță, I. Lesanovsky, and J. P. Garrahan, Phys. Rev. Lett. **116**, 240404 (2016).
- [46] M. B. Plenio and P. L. Knight, Rev. Mod. Phys. **70**, 101 (1998).
- [47] H.-P. Breuer and F. Petruccione, *The Theory of Open Quantum Systems* (Oxford University Press, New York, 2002).
- [48] P. P. Hofer, M. Perarnau-Llobet, L. D. M. Miranda, G. Haack, R. Silva, J. B. Brask, and N. Brunner, New J. Phys. **19**, 123037 (2017).
- [49] F. Ciccarello, Quantum Meas. Quantum Metrol. **4**, 53 (2018).
- [50] S. Choi, J. Choi, R. Landig, G. Kucsko, H. Zhou, J. Isoya, F. Jelezko, S. Onoda, H. Sumiya, V. Khemani, C. Von Keyserlingk, N. Y. Yao, E. Demler, and M. D. Lukin, Nature (London) **543**, 221 (2017).

Supplementary Material for  
*Driven Bose-Hubbard dimer under nonlocal dissipation: A  
bistable time crystal*

C. Lledó,<sup>1,\*</sup> Th. K. Mavrogordatos,<sup>2</sup> and M. H. Szymańska<sup>1</sup>

<sup>1</sup>*Department of Physics and Astronomy,  
University College London, Gower Street,  
London, WC1E 6BT, United Kingdom*

<sup>2</sup>*Department of Physics, Stockholm University, SE-106 91, Stockholm, Sweden*

In the Supplementary Material we provide further details concerning the role of conserved quantities and symmetries in the Bose-Hubbard dimer (BHD), viewed explicitly as an open quantum system. We give further insights on the importance of the conserved swapping operator ( $\hat{Z}_2$ ) in the quantum regime when we approach the first-order *Dissipative Phase Transition* (DPT) of amplitude bistability and its associated metastability. We visualize the quantum fluctuations through the Q-function quasiprobability distribution and quantum-jump trajectories for pump values around the bistability threshold, as the  $N \rightarrow \infty$  thermodynamic limit is approached. We also provide further links to the semiclassical treatment and explain the effective decoupling (between the bonding and antibonding modes) mechanism responsible of the time-crystal behaviour. For all the results in the main text as well as in this analysis, we compare with what is expected from the BHD under *local dissipation*. Moreover, we show how the Lindblad Master Equations (LMEs) with local and nonlocal dissipation can be derived from a total Hamiltonian that includes the environment and its coupling to the BHD. Finally, we explore the possibility of an asymmetric system-environment coupling that destroys the continuous swapping symmetry and the limit cycles in the nonlocal dissipation case. We show that, in spite of this, the Josephson-like oscillations remain long lived, with a robust time-crystalline period.

## CONTENTS

Symmetries and Conserved quantities for a Markovian open quantum system	3
Symmetries and conserved quantities for the BHD	5
Symmetries and conserved quantities in the absence of the nonlinearity	6
Dissipative phase transitions	7
The Gross-Pitaevskii semiclassical equations	9
Local vs nonlocal dissipation	10
Effective antibonding decoupling	14
Emergence of the bistable time crystal in single quantum jump trajectories	15
Local dissipation amplitude bistability	15
Nonlocal dissipation	16



Microscopic derivation of the Lindblad Master Equations	19
Imperfections in the symmetric coupling	23
References	25

## SYMMETRIES AND CONSERVED QUANTITIES FOR A MARKOVIAN OPEN QUANTUM SYSTEM

In order to understand the occurrence of dissipative phase transitions, quantum multi-stability, and quantum limit cycles, it is crucial to investigate the role of symmetries and conserved quantities in open quantum systems, and how these are related to the spectrum of the Liouvillian. We introduce here some analytical properties which we invoke in the main text to appreciate the peculiarities about nonlocal dissipation as opposed to local dissipation.

Let us first introduce the dual super-operator of the Liouvillian. For a general  $\mathcal{L}(\cdot) = -i[\hat{\mathcal{H}}, \cdot] + \sum_k \gamma_k (\hat{L}_k \cdot \hat{L}_k^\dagger - (1/2)\{\hat{L}_k^\dagger \hat{L}_k, \cdot\})$ , its dual

$$\mathcal{L}^*(\cdot) = i[\hat{H}, \cdot] + \sum_k \gamma_k \left( \hat{L}_k^\dagger \cdot \hat{L}_k - \frac{1}{2} \{ \hat{L}_k^\dagger \hat{L}_k, \cdot \} \right) \quad (1)$$

is the generator of the evolution of system operators, i.e.,  $\partial_t \hat{A} = \mathcal{L}^*(\hat{A})$  for any system operator  $\hat{A}$ . It is easy then to show by direct inspection that when the Hamiltonian and every Lindblad operator commutes with an operator  $\hat{O}$ , i.e.,

$$[\hat{H}, \hat{O}] = [\hat{L}_k, \hat{O}] = 0 \quad \forall k, \quad (2)$$

then  $\hat{O}$  is a conserved quantity, with  $\partial_t \hat{O} = \mathcal{L}^*(\hat{O}) = 0$ , and there is a continuous symmetry  $\hat{U}(\phi) = \exp(i\phi\hat{O})$  (for real  $\phi$ ) such that  $\mathcal{L}(\hat{U}(\phi)\hat{\rho}\hat{U}(\phi)^\dagger) = \hat{U}(\phi)\mathcal{L}(\hat{\rho})\hat{U}(\phi)^\dagger$  for any  $\hat{\rho}$ . This is a one way implication only ( $\Rightarrow$ ). Examples which show that this is not an equivalence and that a continuous symmetry does not necessarily have a conserved quantity and *vice versa* can be found in [1].

In general, the Liouvillian  $\mathcal{L}$  can be subject to a spectral decomposition. (An equivalent formulation of these statements in the so-called *Liouville space* can be found in [1]). Let us consider the set of operators  $\{\hat{r}_{n,d_n}, \hat{l}_{n,d_n}\}$  which are eigenoperators of the Liouvillian  $\mathcal{L}$  and its dual  $\mathcal{L}^*$ :

$$\mathcal{L}(\hat{r}_{n,d_n}) = \lambda_n \hat{r}_{n,d_n}, \quad \mathcal{L}^*(\hat{l}_{n,d_n}) = \lambda_n^* \hat{l}_{n,d_n}, \quad (3)$$

and are orthonormal in the internal *Hilbert-Schmidt* dot product

$$\text{Tr}[\hat{l}_{j,d_j}^\dagger \hat{r}_{k,d_k}] = \delta_{jk} \delta_{d_j, d_k}, \quad (4)$$

where the sub-index  $d_n = 1, 2, 3, \dots$  labels the degeneracy of the eigenvalue  $\lambda_n$ . The set of operators  $\{\hat{r}_{n,d_n}, \hat{l}_{n,d_n}\}$  form a basis of bounded operators in the system Hilbert space, thus the solution of the Lindblad equation  $\hat{\rho}(t) = e^{t\mathcal{L}}\hat{\rho}(0)$  can be expanded as

$$\hat{\rho}(t) = \sum_{n,d_n} c_{n,d_n} e^{t\mathcal{L}} \hat{r}_{n,d_n} = \sum_{n,d_n} c_{n,d_n} e^{t\lambda_n} \hat{r}_{n,d_n}, \quad (5)$$

with complex coefficients

$$c_{n,d_n} = \text{Tr}[\hat{l}_{n,d_n}^\dagger \hat{\rho}(0)], \quad (6)$$

depending on the initial condition. Note that  $\hat{r}_{n,d_n}$  and  $\hat{l}_{n,d_n}$  are not necessarily density matrices, in the sense that they might not be semidefinite positive, hermitian, or have a unit trace.

Since in general the Liouvillian is not the same as its dual, the eigenvalues  $\lambda_n$  are complex. It becomes clear from Eq. (5) that in order to describe a physical evolution (a *CPTP map*) they must have nonnegative real parts,  $\text{Re}[\lambda_n] \leq 0$ , or else the density matrix would grow exponentially in time. This means that their real parts are decay rates while their imaginary parts give rise to oscillations. We can order them such that  $0 \geq \text{Re}(\lambda_0) \geq \text{Re}(\lambda_1) \geq \text{Re}(\lambda_2) \geq \dots$ . There is always an eigenvalue equal to zero ( $\lambda_0 = 0$ ) since the identity satisfies  $\mathcal{L}^*(\hat{\mathbb{1}}) = 0$ . This is due to the trace-preserving condition of the evolution. In other words, the identity is trivially conserved. If the identity is the only conserved operator and there is no other purely imaginary eigenvalue, then the steady state of Eq.(5) assumes the form

$$\hat{\rho}_{\text{ss}} = \lim_{t \rightarrow \infty} \hat{\rho}(t) = c_{0,1} \hat{r}_{0,1} = \hat{r}_{0,1}, \quad (7)$$

since  $c_{0,1} = \text{Tr}[\hat{\mathbb{1}}\hat{\rho}(0)] = \text{Tr}[\hat{\rho}(0)] = 1$ . This steady state is unique and carries no information about the initial condition. We note that, as proved in [2], for any finite Hilbert space cutoff, all systems with local bosonic Lindblad operators of the form  $\hat{a}_i$  acting on the mode (or site)  $i$ , possess a unique steady state or, equivalently, cannot have any nontrivial conserved operator. This is the case of the local dissipation for the BHD that is most commonly considered in the literature (see e.g. [3, 4]).

If there is, however, a nontrivial conserved operator  $\hat{O}$ , then the steady state will take the form

$$\hat{\rho}_{\text{ss}} = \hat{r}_{0,1} + c_{0,2} \hat{r}_{0,2}, \quad (8)$$

where the coefficient  $c_{0,2} = \text{Tr}[\hat{O}^\dagger \hat{\rho}(0)]$  preserves some information of the initial condition. The infinite number of possible steady states is a direct consequence of the presence of a nontrivial conserved quantity. Note that the following orthonormality conditions hold:

$$\begin{aligned}
1 &= \text{Tr}[\hat{\mathbb{1}}\hat{r}_{0,1}] = \text{Tr}[\hat{r}_{0,1}], \\
0 &= \text{Tr}[\hat{\mathbb{1}}\hat{r}_{0,2}] = \text{Tr}[\hat{r}_{0,2}], \\
0 &= \text{Tr}[\hat{O}^\dagger \hat{r}_{0,1}], \\
1 &= \text{Tr}[\hat{O}^\dagger \hat{r}_{0,2}].
\end{aligned} \tag{9}$$

In particular, an initial condition can be chosen such that  $c_{0,2} = 0$ , thus  $\hat{r}_{0,1}$  is always a density matrix.

It is possible to have a purely imaginary eigenvalue (together with its complex conjugate), for instance  $\lambda_1 = i\text{Im}[\lambda_1]$  (and  $\lambda_1^* = -i\text{Im}[\lambda_1]$ ), which would give rise to a quantum limit cycle [5]. If there are no conserved quantities (besides the identity), in the long-time limit, the steady state will have the oscillatory form

$$\hat{\rho}_{\text{ss}}(t) = \hat{r}_{0,1} + c_{1,1}e^{\lambda_1 t}\hat{r}_{1,1} + c_{1,1}^*e^{\lambda_1^* t}\hat{r}_{1,1}^\dagger, \tag{10}$$

with  $c_{1,1} = \text{Tr}[\hat{l}_{1,1}^\dagger \hat{\rho}(0)]$ .

### Symmetries and conserved quantities for the BHD

The local dissipation Liouvillian  $\mathcal{L}_{\text{loc}}(\cdot) = -i[\hat{\mathcal{H}}, \cdot] + \gamma\mathcal{D}[\hat{a}_1](\cdot) + \gamma\mathcal{D}[\hat{a}_2](\cdot)$ , with the Hamiltonian  $\hat{\mathcal{H}}$  of the BHD given in Eq.(2) in the main text, has a discrete  $Z_2$  symmetry,  $\hat{a}_1 \leftrightarrow \hat{a}_2$ , which can be readily checked by inspection. Formally, this is given by the unitary swapping operator  $\hat{Z}_2 = \sum_{n_1, n_2} |n_1, n_2\rangle \langle n_2, n_1|$ , written in the Fock-state basis of the two modes (with  $n_1, n_2$  their occupation number). Then, using the fact that  $\hat{Z}_2\hat{a}_1\hat{Z}_2 = \hat{a}_2$  and  $\hat{Z}_2\hat{a}_2\hat{Z}_2 = \hat{a}_1$  (note that  $\hat{Z}_2^{-1} = \hat{Z}_2$ ), one can check that

$$\mathcal{L}_{\text{loc}}(\hat{Z}_2\hat{\rho}\hat{Z}_2) = \hat{Z}_2\mathcal{L}_{\text{loc}}(\hat{\rho})\hat{Z}_2. \tag{11}$$

Since  $\partial_t \hat{\rho} = \mathcal{L}_{\text{loc}}(\hat{\rho})$  has a unique steady state [2], it follows that  $\hat{\rho}_{\text{ss}}^{\text{loc}} = \hat{Z}_2\hat{\rho}_{\text{ss}}^{\text{loc}}\hat{Z}_2$ ; hence, if one traces out any of the two modes the density matrix remains the same:

$$\hat{\rho}_{\text{ss},1}^{\text{loc}} = \text{Tr}_2[\hat{\rho}_{\text{ss}}^{\text{loc}}] = \text{Tr}_1[\hat{\rho}_{\text{ss}}^{\text{loc}}] = \hat{\rho}_{\text{ss},2}^{\text{loc}}. \tag{12}$$

Note that this is only a discrete symmetry and no continuous symmetry can be generated by  $\hat{Z}_2$  since it does not commute with both Lindblad operators  $\hat{a}_1$  and  $\hat{a}_2$  individually.

For the nonlocal dissipation case, since  $\hat{Z}_2$  commutes with the Hamiltonian and with the unique Lindblad operator  $(\hat{a}_1 + \hat{a}_2)$ , the symmetry is continuous and  $\hat{Z}_2$  is conserved, thus,

$$\mathcal{L}(\hat{U}(\phi)\hat{\rho}\hat{U}(\phi)^\dagger) = \hat{U}(\phi)\mathcal{L}(\hat{\rho})\hat{U}(\phi)^\dagger \quad \text{and} \quad \partial_t \hat{Z}_2 = 0, \quad (13)$$

with  $\hat{U}(\phi) = e^{i\phi\hat{Z}_2} = \cos(\phi)\hat{1} + i\sin(\phi)\hat{Z}_2$ . As stated in the main text, the steady state  $\hat{\rho}_{\text{ss}}$  is always symmetric independently of the initial condition for any finite system size  $N$ . This is not necessarily true when the  $\lambda_0 = 0$  eigenvalue becomes degenerated in the thermodynamic limit, where a spontaneous symmetry breaking can take place.

### Symmetries and conserved quantities in the absence of the nonlinearity

An alternative representation that is helpful to understand the difference between the local and nonlocal dissipation approaches is obtained by rewriting the Liouvillians  $\mathcal{L}$  and  $\mathcal{L}_{\text{loc}}$  in terms of the bonding and anti-bonding bosonic operators  $\hat{a}_{B,A} = (\hat{a}_1 \pm \hat{a}_2)/\sqrt{2}$ , respectively. The Hamiltonian of Eq. (1) in the main text becomes

$$\begin{aligned} \hat{\mathcal{H}} = & (-\Delta - J)\hat{a}_B^\dagger\hat{a}_B + (-\Delta + J)\hat{a}_A^\dagger\hat{a}_A + \sqrt{2}F(\hat{a}_B^\dagger + \hat{a}_B) \\ & + \frac{U}{4} \left[ \sum_{k=B,A} (\hat{a}_k^\dagger\hat{a}_k^\dagger\hat{a}_k\hat{a}_k) + 2\hat{a}_B^\dagger\hat{a}_B^\dagger\hat{a}_A\hat{a}_A + 2\hat{a}_B\hat{a}_B\hat{a}_A^\dagger\hat{a}_A^\dagger \right. \\ & \left. + 8\hat{a}_B^\dagger\hat{a}_B\hat{a}_A^\dagger\hat{a}_A \right]. \end{aligned} \quad (14)$$

The local dissipator  $\mathcal{D}_{\text{loc}}(\cdot) = \gamma\mathcal{D}[\hat{a}_1](\cdot) + \gamma\mathcal{D}[\hat{a}_2](\cdot)$  is rewritten as

$$\mathcal{D}_{\text{loc}}(\cdot) = \gamma\mathcal{D}[\hat{a}_B](\cdot) + \gamma\mathcal{D}[\hat{a}_A](\cdot), \quad (15)$$

while the nonlocal dissipator  $\mathcal{D}(\cdot) = \gamma\mathcal{D}[\hat{a}_1 + \hat{a}_2](\cdot)$  is

$$\mathcal{D}(\cdot) = 2\gamma\mathcal{D}[\hat{a}_B](\cdot). \quad (16)$$

We note that in the Hamiltonian of Eq. (14) the driving changes only the occupation of the bonding mode, while the nonlinear terms couple the bonding and antibonding modes. This means that if we remove the nonlinearity ( $U = 0$ ), we have that the Hamiltonian conserves the antibonding mode occupation number  $[\hat{\mathcal{H}}_{\text{linear}}, \hat{n}_A] = 0$  where  $\hat{n}_A = \hat{a}_A^\dagger\hat{a}_A$ . While

both modes are dissipated in the local approach, only the bonding mode is dissipated in the nonlocal approach, which means that  $\hat{n}_A$  is a conserved operator when the dissipation is nonlocal,  $\partial_t \hat{n}_A = \mathcal{L}_{\text{linear}}^*(\hat{n}_A) = 0$ , and is associated with a continuous antibonding rotation symmetry given by the unitary transformation  $\hat{R} = e^{i\theta \hat{n}_A}$  (for real  $\theta$ ). For the local dissipation approach, the antibonding mode is dissipated such that  $\hat{n}_A$  is not a conserved quantity, even though  $\hat{R}$  defines a continuous symmetry, i.e.,  $\mathcal{L}_{\text{loc}}(\hat{R}\hat{\rho}\hat{R}^\dagger) = \hat{R}\mathcal{L}_{\text{loc}}(\hat{\rho})\hat{R}^\dagger$ . Since  $\hat{1}$ ,  $\hat{Z}_2$ , and  $\hat{n}_A$  are linearly independent, we conclude that in the absence of the nonlinearity there are three conserved quantities in the nonlocal approach when driving is symmetric ( $F_1 = F_2$ ).

Note that the bonding and antibonding modes are completely decoupled in the dynamics if  $U = 0$ . Under local dissipation the antibonding mode is damped due to the dissipation, whereas under nonlocal dissipation the antibonding mode evolves coherently (i.e. without dissipation) as we mention in the main text. This means there is a purely imaginary Liouvillian eigenvalue ( $\lambda = i(J - \Delta)$ ) responsible for trivial coherent oscillations. As we discuss later, this decoupling is essential to our understanding of the emergence of limit cycles in the BHD as an effective decoupling between the bonding and antibonding modes [6].

In principle, there could be other conserved quantities in the local or nonlocal dissipation cases. However, by numerically calculating the degeneracy of the zero eigenvalue, one can check that for local dissipation there is only one conserved quantity (the identity) while for the nonlocal case, one has two conserved quantities ( $\hat{1}$  and  $\hat{Z}_2$ ) in the presence of the nonlinearity, and an additional one ( $\hat{n}_A$ ) when the nonlinearity is removed. There could be other continuous symmetries we are not aware of, but these would not be associated with conserved quantities.

We also remark that the zero eigenvalue corresponding to the conserved operator  $\hat{n}_A$  in the nonlocal dissipation case might be absent in a numerically-obtained spectral decomposition of  $\mathcal{L}_{\text{linear}}$  because  $\hat{n}_A$  does not commute with  $\hat{\mathcal{H}}$  or  $\hat{a}_B$  for a finite Hilbert-space cutoff. This is not the case for  $\hat{Z}_2$ , which commutes with both operators for any cutoff.

## DISSIPATIVE PHASE TRANSITIONS

It is a well-known fact that, due to the nonlinearity, the semiclassical regime of the BHD with local dissipation can present bistability (for symmetric driving) [7] or undergo a

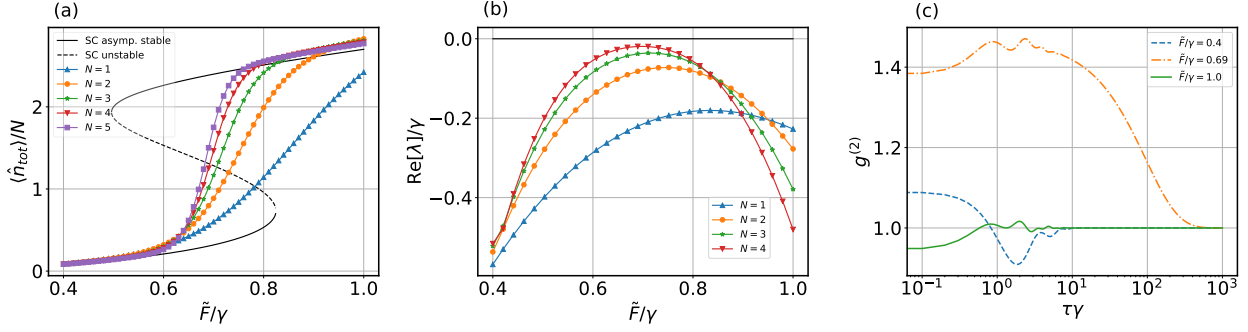


FIG. 1. **Bistability for local dissipation.** Frames (a) and (b) show the total number of bosons  $\langle \hat{n}_{\text{tot}} \rangle / N$  in the steady state and the real part of the Liouvillian gap,  $\text{Re}[\lambda]/\gamma$ , respectively, as a function of the scaled drive  $\tilde{F}/\gamma = N^{-1/2}F/\gamma$  for different values of  $N$ . In (a) the black solid and dashed lines, denoted in the legend by *SC*, depict semiclassical calculations. Frame (c) shows the time-delayed second-order coherence function  $g^{(2)}(\tau\gamma)$  for three different pump values and  $N = 5$ . The parameters used read:  $\Delta = J = \tilde{U} = \gamma$  and  $U = \tilde{U}/N$ .

symmetry breaking (for anti-symmetric driving)[4] in the steady state, as a scaled system parameter is varied. These two phenomena are associated with dissipative phase transitions. In analogy with a *closed* quantum system, where the excitation gap of the Hamiltonian in the thermodynamic limit may close when a parameter is varied, in an *open* quantum system the spectrum gap of the Liouvillian ( $\mathcal{L}$ ) may also close for an appropriately-defined thermodynamic limit. In the former case, the transition is termed *quantum phase transition*, while in the latter, *dissipative phase transition* (DPT) [8, 9].

In simple words, if the gap in the Liouvillian spectrum, i.e., the eigenvalue  $\lambda \equiv \lambda_1$ , tends towards zero in the thermodynamic limit for either a specific value of a varying parameter ( $\xi = \xi_c$ ) or in a whole region of  $\xi \in \Xi$ , then a *first-order* or *second-order* DPT may occur. Since  $\text{Re}[\lambda]$  is the smallest decay rate, the system response exhibits a *critical slowing down* as that rate approaches zero, which means that it takes a very long time ( $\sim \text{Re}[\lambda]^{-1}$ ) to reach the steady state. This behaviour has been observed experimentally in photon time-delayed correlation measurements in single cavity polaritons [10]. The difference between the DPTs of first and second order is that in the former there is a nonanalyticity at the single critical point  $\xi_c$  due to a level crossing, while in the latter the eigenoperator associated with the eigenvalue of the closing gap renders the steady-state subspace degenerated [9], hence subject to energy-costless excitations that break the symmetry (i.e., Goldstone modes).

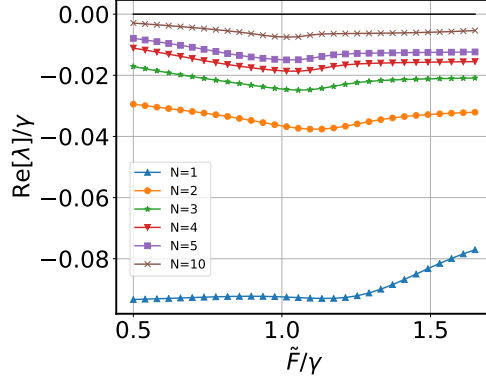


FIG. 2. **First Liouvillian gap for nonlocal dissipation** as a function of the scaled drive  $\tilde{F}/\gamma = N^{-1/2}F/\gamma$  for  $N = [1 - 5, 10]$ . The parameters used read:  $\Delta/\gamma = 0.7$ ,  $J = 1.5$ ,  $\tilde{U}/\gamma = 1.0$  and  $U = \tilde{U}/N$ .

In the following subsection, we spend some time on the semiclassical results derived from our model, and explain the relevance to the quantum picture.

### The Gross-Pitaevskii semiclassical equations

Starting from the LME for local or nonlocal dissipation, a semiclassical approximation can be obtained by computing  $\text{Tr}[\hat{a}_i \partial_t \hat{\rho}]$  assuming that the state of the system is uncorrelated and coherent, with a density matrix of the form  $\hat{\rho} = |\alpha_1, \alpha_2\rangle \langle \alpha_1, \alpha_2|$ . One then obtains two coupled nonlinear differential equations for the complex-field amplitudes:

$$\begin{aligned} i\partial_t \alpha_1 &= (-\Delta - i\gamma/2 + 2U|\alpha_1|^2)\alpha_1 - (J + i\epsilon\gamma/2)\alpha_2 + F, \\ i\partial_t \alpha_2 &= (-\Delta - i\gamma/2 + 2U|\alpha_2|^2)\alpha_2 - (J + i\epsilon\gamma/2)\alpha_1 + F, \end{aligned} \quad (17)$$

where  $\epsilon = 0$  ( $\epsilon = 1$ ) is for local (nonlocal) dissipation. With the scaling introduced in the main text, the coupled equations (17) become

$$\begin{aligned} i\partial_t \tilde{\alpha}_1 &= (-\Delta - i\gamma/2 + 2\tilde{U}|\tilde{\alpha}_1|^2)\tilde{\alpha}_1 - (J + i\epsilon\gamma/2)\tilde{\alpha}_2 + \tilde{F}, \\ i\partial_t \tilde{\alpha}_2 &= (-\Delta - i\gamma/2 + 2\tilde{U}|\tilde{\alpha}_2|^2)\tilde{\alpha}_2 - (J + i\epsilon\gamma/2)\tilde{\alpha}_1 + \tilde{F}. \end{aligned} \quad (18)$$

Here we have rescaled the complex amplitudes as  $\alpha_i = \sqrt{N}\tilde{\alpha}_i$ . These equations are valid for any  $N$ . In particular, as  $N \rightarrow \infty$  the number of particles diverges as  $|\alpha_i|^2 = |\tilde{\alpha}_i|^2 N \rightarrow \infty$ . We remark that  $N$  is an unphysical parameter conveniently introduced to define a weak-coupling thermodynamic limit, and is not related to the total number of particles itself.

We note that in the so-called *weak-lasing* regime of exciton-polaritons [11], equations similar to Eq.(17) are used, where two coupled Bose-Einstein condensation centers are described by their mean-field order parameters, under collective dissipation. It has been shown that such a model has limit cycles [12]. The main difference with our semiclassical model is that in our case the pump is coherent, while weak-lasing occurs under incoherent pump.

The semiclassical equations (18) are accompanied by their complex conjugates. We therefore introduce the compact vector notation

$$\partial_t \tilde{\boldsymbol{\alpha}}(t) = \mathbf{G}(\tilde{\boldsymbol{\alpha}}), \quad \tilde{\boldsymbol{\alpha}}(t) = \begin{pmatrix} \tilde{\alpha}_1(t) \\ \tilde{\alpha}_1^*(t) \\ \tilde{\alpha}_2(t) \\ \tilde{\alpha}_2^*(t) \end{pmatrix}, \quad (19)$$

where  $\mathbf{G}$  is the vector field that depends nonlinearly on the  $\tilde{\alpha}_i$ . We investigate numerically the stationary solutions  $\tilde{\boldsymbol{\alpha}}(t) = \tilde{\boldsymbol{\alpha}}$  of the system defined by Eq. (19). We then analyze their stability by expanding the vector  $\tilde{\boldsymbol{\alpha}}$  around the stationary solutions up to first order in the fluctuations, obtaining a linear first-order differential equation for the fluctuation vector  $\boldsymbol{\delta}(t) = (\delta_1(t), \delta_1^*(t), \delta_2(t), \delta_2^*(t))^T$ :

$$\partial_t \boldsymbol{\delta}(t) = \mathbf{M} \boldsymbol{\delta}(t), \quad (20)$$

where  $\mathbf{M} = \partial \mathbf{G} / \partial \tilde{\boldsymbol{\alpha}}$  is the Jacobian matrix evaluated for the steady-state solution under consideration.

The Jacobian  $4 \times 4$  matrix  $\mathbf{M}$  generally has complex eigenvalues  $\{w_j\}_{j=1}^4$ . If any of the four eigenvalues has a positive real part, the solution is *unstable*, as the fluctuations will grow exponentially with time. If all of them have nonpositive real parts, ( $\text{Re } w_j \leq 0$ ), the solution is *stable*, while if they all have negative real part ( $\text{Re } w_j < 0$ ), the solution is called *asymptotically stable*. The difference between these last two is that only in the latter every fluctuation due to a perturbation decays in time. For some parameters values, we have also integrated Eq. (19) in time to probe the presence of a limit cycle (i.e., a periodic orbit in the phase portrait reached in the long-time limit).

## LOCAL VS NONLOCAL DISSIPATION

In this Section, we discuss the differences arising between the semiclassical and the quantum description for local and nonlocal dissipation.



The BHD with local dissipation exhibits semiclassical bistability. In Fig. 1(a) we show the rescaled total number of excitations in the system,  $\langle \hat{n}_{\text{tot}} \rangle / N = (\langle \hat{a}_1^\dagger \hat{a}_1 \rangle + \langle \hat{a}_2^\dagger \hat{a}_2 \rangle) / N$  (which in the semiclassical approximation corresponds to  $|\tilde{\alpha}_1|^2 + |\tilde{\alpha}_2|^2$ ) as a function of the rescaled pump amplitude  $\tilde{F} / \gamma = F / (\sqrt{N} \gamma)$ . The black solid lines are two branches of asymptotically-stable fixed points while the black dashed line is an unstable branch. There is a pump amplitude window in which two asymptotically stable solutions are allowed. For a given initial condition the response reach either one or the other, which is the cause of hysteresis cycles if one is to ramp the pump up and down as in [13]. The basin of attraction of these asymptotically stable solutions (i.e., the set of initial-condition points which asymptotically converge with time into the given fixed point) appears to be the complete two-dimensional complex space  $\mathbb{C}^2$  (or four-dimensional real space), as all the initial conditions we have tried converge to the corresponding fixed point, as shown in Fig. 1(a) (or, in the region of bistability, to one of the two fixed points). We also show the total number of bosons in the quantum regime for different values of  $N$ . Similarly to the case of nonlocal dissipation (see Fig. 1(a) in the main text), one can see that as  $N$  increases, the occupation number approaches one of the two semiclassical stable branches.

Besides the absence of limit cycles in the local dissipation approach, another important difference in this approach is that there is only a first-order DPT and no symmetry breaking. In Fig. 1(b) we show the Liouvillian ( $\mathcal{L}_{\text{loc}}$ ) gap as a function of the rescaled pump amplitude for different values of  $N$  (its imaginary part is zero for all pump values we consider). This should be contrasted with the first gap of the Liouvillian in the nonlocal approach shown in Fig. 1(c) in the main text, which we have also plotted here in Fig. 2 for higher values of  $N$ . In the local case, it only closes asymptotically at the bistability threshold. The first gap of  $\mathcal{L}_{\text{loc}}$  has a negative-parabola shape, similar to the eigenvalue at medium pump shown in Fig. 1(c) in the main text for nonlocal dissipation, which we ascribe responsible of the bistability. We remark that the second gap of  $\mathcal{L}_{\text{loc}}$  (not shown) approaches a finite real value as  $N$  increases, thus no limit cycles can be formed. In Fig. 1(c) we show the time-delayed second-order coherence function  $g^{(2)}(\tau\gamma)$  (defined in the main text) for local dissipation. We consider pump values before, inside, and above the bistability region. It is clear that the critical slowing down only occurs at the bistability threshold (orange dashed-line), as expected from the smallness of the Liouvillian gap in this region (see Fig. 1(b)). A clear manifestation that in this case the steady state is unique is that, for the three pump values,

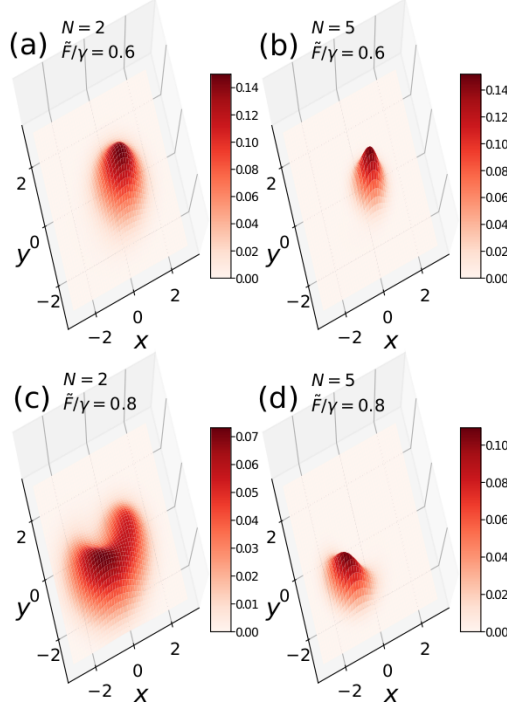


FIG. 3. **Rescaled Q-functions for local dissipation** below ( $\tilde{F}/\gamma = 0.6$ ) and above ( $\tilde{F}/\gamma = 0.8$ ) the bistability threshold for two values of  $N$ . The axes are  $(x, y) = (\text{Re } \alpha, \text{Im } \alpha)/\sqrt{N}$ . All the other parameters are the same as in Fig. 1.

at long times the system relaxes to a steady state which is the same to the starting one ( $g^{(2)} \rightarrow 1$ ).

An alternative way of ascertaining the presence of quantum bistability is through a quasiprobability distribution in the phase space. In Fig. 3 we plot the (rescaled) Q-function  $Q(\tilde{\alpha}) = \langle \tilde{\alpha} | \hat{\rho}_{\text{ss}} | \tilde{\alpha} \rangle / \pi$  under local dissipation for two values of  $N$  and two pump values, one below [(a) and (b)] and one above [(c) and (d)] the bistability threshold. Below threshold only one peak is observed, while above threshold a transition from a dark to a bright state begins at  $N = 2$ , to reach completion for  $N = 5$ .

We now proceed to calculate the Q-function corresponding to the steady state reached when the dissipation is nonlocal. In this case, the steady state has the form of Eq. (8) with the conserved operator  $\hat{O} = \hat{Z}_2$ . Since the eigenvalues of  $Z_2$  are  $\pm 1$ , the expectation value  $\langle \hat{Z}_2 \rangle$  for any density matrix is bounded between  $-1$  and  $+1$ . In Fig. 4 we plot the rescaled Q-function corresponding to  $\hat{r}_{0,1}$  [(a-d)] and  $\hat{r}_{0,2}$  [(e-h)], for increasing values of  $N$  and two pump strengths, one below ( $\tilde{F}/\gamma = 0.8$ ) and one above ( $\tilde{F}/\gamma = 1.3$ ) the bistability

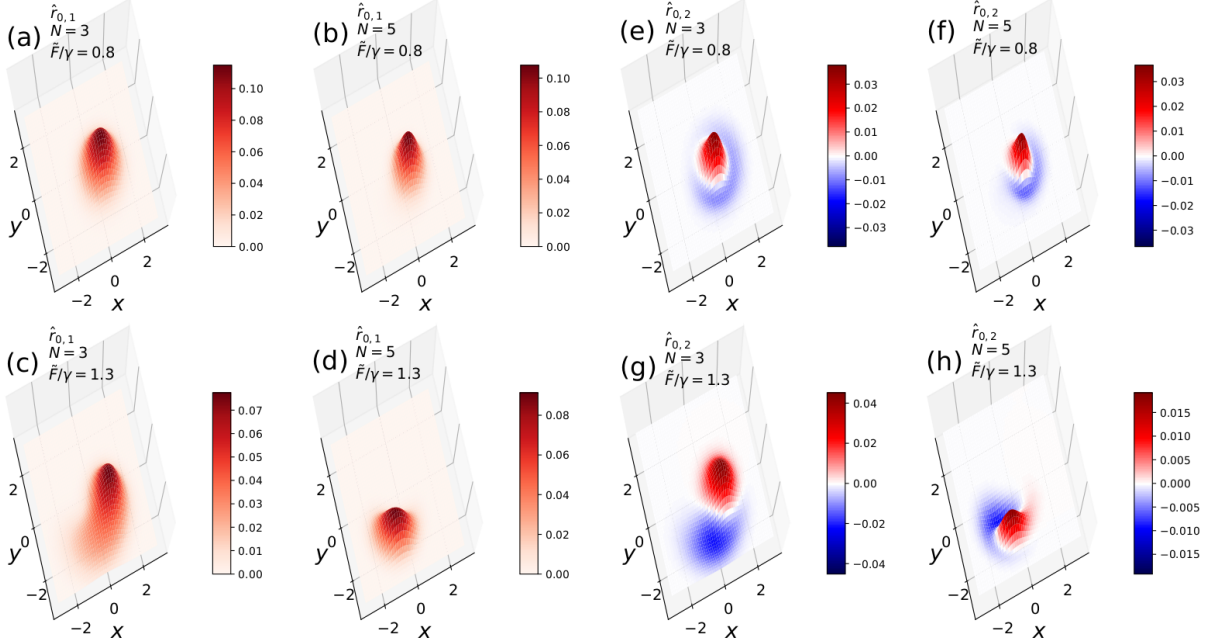


FIG. 4. **Rescaled Q-functions** corresponding to the two zero-eigenvalue eigenoperators of  $\mathcal{L}$  that lead to the steady state **for nonlocal dissipation**. The steady state has the form of Eq. (8), with  $c_{0,2} = \text{Tr}[\hat{Z}_2 \hat{\rho}(0)]$ . Here  $\hat{r}_{0,1}$  (a-d) is a density matrix while  $\hat{r}_{0,2}$  (e-h) is not. The Q-functions are plotted for two values of  $N$ , and two pump amplitudes: one below ( $\tilde{F}/\gamma = 0.8$ ) and one above ( $\tilde{F}/\gamma = 1.3$ ) threshold. The axes are  $(x, y) = (\text{Re } \alpha, \text{Im } \alpha)/\sqrt{N}$ . All the other parameters are the same as in Fig. 2 (and Fig. 1 in the main text).

threshold. Any initial condition will lead to a linear combination of these two Q-functions in the steady state. The Q-function of  $\hat{r}_{0,1}$  shows a very similar behavior to the one for local dissipation in Fig. 3. The Q-function of  $\hat{r}_{0,2}$ , instead, takes also negative values in some regions (depicted in blue color) since it does not correspond to a density matrix.

As one can deduce from the plots for  $N = 3$  and  $\tilde{F}/\gamma = 1.3$ , when  $\hat{\rho}_{\text{ss}} = \hat{r}_{0,1} + \hat{r}_{0,2}$ , the Q-function of  $\hat{r}_{0,2}$  will add some occupation probability to the dark state, while subtracting some from the bright state, in such a way that the transition will be observed for larger  $N$ . If instead one selects  $\hat{\rho}_{\text{ss}} = \hat{r}_{0,1} - \hat{r}_{0,2}$ , the transition will be accomplished for lower  $N$ . Interestingly, however, the participation of the Q-function corresponding to  $\hat{r}_{0,2}$  fades away with increasing  $N$  for high pump values, suggesting that in the thermodynamic limit the choice of initial condition for  $c_{0,2}$  is unimportant above threshold. The initial condition will be important, however, for other eigenmodes of gaps that close in the thermodynamic limit,

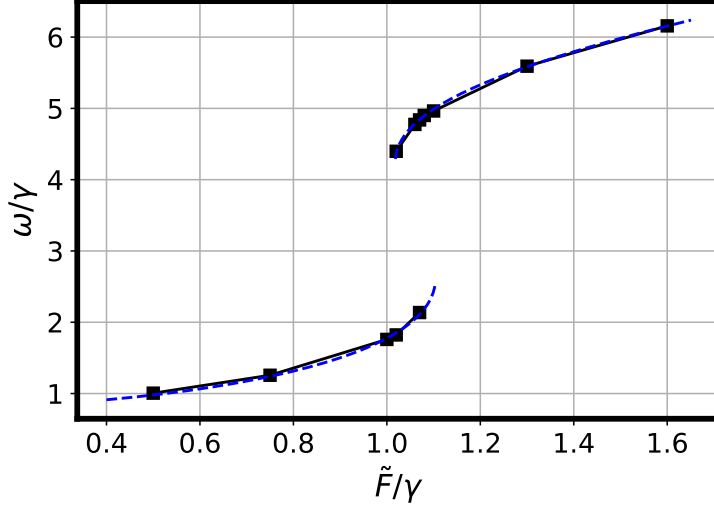


FIG. 5. **Semiclassical limit-cycle frequency as a function of the rescaled pump amplitude.** Black squares are calculated by time-integrating Eq. (18), also shown in Fig. 1(c) in the main text. The dashed blue line is the effective frequency given in Eq. (22) after the decoupling approximation. Same parameters as in Fig. 2 (and Fig. 1 in the main text).

as well as for the eigenmodes associated to the limit cycles discussed in the main text.

## EFFECTIVE ANTIBONDING DECOUPLING

The mechanism responsible for the emergence of limit cycles and the time-crystalline behaviour is an effective decoupling between the bonding and antibonding mode. As we have discussed in the main text, when the antibonding mode population is sufficiently small such that  $|\tilde{\alpha}_A|^2 \equiv |\tilde{\alpha}_1 - \tilde{\alpha}_2|^2/2 \ll 1$ , bonding and antibonding modes are effectively decoupled in the semiclassical equations of motion.

In order to appreciate this decoupling we start by writing the semiclassical equations for the bonding and antibonding modes:

$$\begin{aligned}
 i\partial_t \tilde{\alpha}_B &= (-\Delta - J - i\gamma)\tilde{\alpha}_B + \frac{\tilde{U}}{2}(|\tilde{\alpha}_B|^2 \tilde{\alpha}_B + 2\tilde{\alpha}_A^2 \tilde{\alpha}_B^* + 4|\tilde{\alpha}_A|^2 \tilde{\alpha}_B) + \sqrt{2}\tilde{F} \\
 i\partial_t \tilde{\alpha}_A &= (-\Delta + J)\tilde{\alpha}_A + \frac{\tilde{U}}{2}(|\tilde{\alpha}_A|^2 \tilde{\alpha}_A + 2\tilde{\alpha}_B^2 \tilde{\alpha}_A^* + 4|\tilde{\alpha}_B|^2 \tilde{\alpha}_A).
 \end{aligned}
 \tag{21}$$

As the state of the system slowly approaches the stable steady states (shown in Fig. 1(a) in the main text), the antibonding mode  $\tilde{\alpha}_A$  becomes small. Neglecting quadratic terms in

$\tilde{\alpha}_A$  decouples the two equations 21. At the same time, the antibonding evolution becomes linear in  $\tilde{\alpha}_A$  and the bonding mode enters as an energy-renormalization term. Solving the linear antibonding mode equation (and its complex conjugate) gives two eigenvalues that correspond to the oscillation frequency of the limit cycles:

$$\omega_{\pm} = \pm \sqrt{(-\Delta + J + 2\tilde{U}|\tilde{\alpha}_B|^2)^2 - \tilde{U}^2|\tilde{\alpha}_B|^4}, \quad (22)$$

which are always real for the parameters we use in our work [ $(J - \Delta)/\gamma = 0.8 > 0$ ]. In Fig. 5 we compare the limit-cycle frequencies (squares) shown in Fig. 1(c) in the main text, with the effective frequency (dashed line) obtained in Eq. (22) using the stable steady state solutions of Eq. (18) to evaluate  $\tilde{\alpha}_B$ . The agreement is perfect.

## EMERGENCE OF THE BISTABLE TIME CRYSTAL IN SINGLE QUANTUM JUMP TRAJECTORIES

### Local dissipation amplitude bistability

An important consequence of bistability is that in single experimental realisations, the system spends long times in either of two metastable states [14], switching between them with a rate much smaller than all other times scales in the system. This can be studied calculating single quantum jump Monte-Carlo trajectories [15] for pump values inside the bistability threshold. In 6 we show a typical single trajectory for a BHD with local dissipation at the bistability threshold ( $\tilde{F}/\gamma = 0.68$ ) for two values of  $N$ . In the top panel, we observe that as  $N$  increases, the rescaled total number of bosons starts to fluctuate around two *metastable* values, switching between them at a rate which is much smaller than the system decay rate (for  $N = 10$  the switching rate is  $\sim 10^{-3}\gamma$ ). The metastable states are associated with the dark and bright states of amplitude bistability. This can be seen in the time evolution of the bonding mode in phase space shown at the bottom of the figure. The anti-bonding mode, instead, fluctuates around zero due to the swapping symmetry of the configuration, but the fluctuations decrease in size with growing  $N$ .

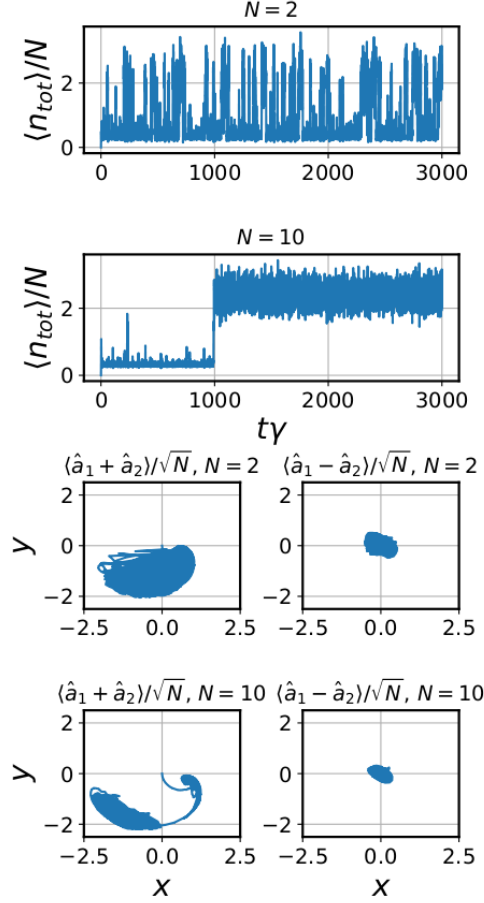


FIG. 6. **Single quantum trajectory for local dissipation at the bistability threshold** ( $\tilde{F}/\gamma = 0.68$ ) for two values of  $N$ . We show the rescaled total number of bosons as a function of time at the top, and the rescaled bonding and antibonding modes evolution in phase space at the bottom. In the latter, the axis are  $(x, y) = (\text{Re}(\alpha_1 \pm \alpha_2), \text{Im}(\alpha_1 \pm \alpha_2))\sqrt{N}$ . All the other parameters are the same as in Fig. 1.

### Nonlocal dissipation

In the case of nonlocal dissipation, both the emergence of the time crystal and of bistability can be observed in single quantum trajectories.

Knowing that the swapping operator  $\hat{Z}_2$  commutes with the BHD Hamiltonian and the nonlocal Lindblad operator  $\hat{a}_1 + \hat{a}_2$ , one can easily verify the following statement: if at any time  $t = \tau$  during the quantum jump Monte-Carlo evolution the pure state  $|\psi(t)\rangle$  becomes either symmetric or antisymmetric under the action of  $\hat{Z}_2$ , such that  $\hat{Z}_2 |\psi(\tau)\rangle = \pm |\psi(\tau)\rangle$ , then **(i)** for all consecutive times  $t \geq \tau$  the expectation value of  $\hat{Z}_2$  remains the same, and

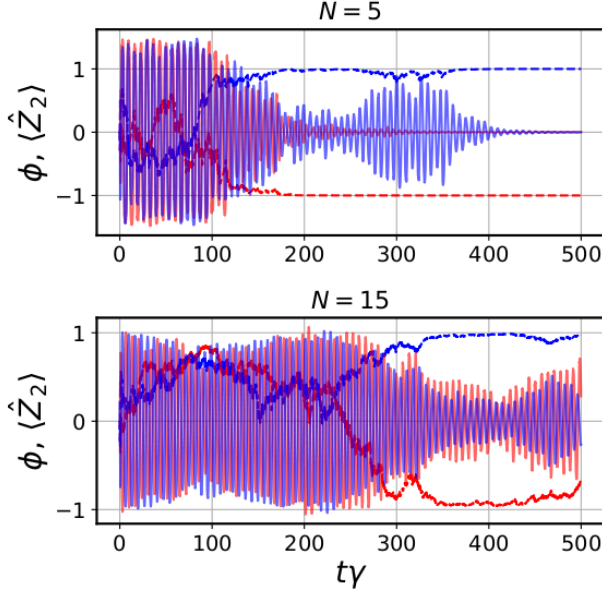


FIG. 7. **Dynamical evolution in single quantum trajectories for nonlocal dissipation.** Relative phase  $\phi = \text{Arg}[\langle \hat{a}_1 \rangle] - \text{Arg}[\langle \hat{a}_2 \rangle]$  (solid line) and  $\langle \hat{Z}_2 \rangle$  (dashed line) as a function of time for two values of  $N$  and  $|\psi(0)\rangle = |0, 1\rangle$ . Same parameters as in Fig. 2 (and Fig. 1 in the main text).

(ii) the expectation value of the anti-bonding mode  $(\hat{a}_1 - \hat{a}_2)/\sqrt{2}$  is zero —that is,

$$\langle \psi(t) | \hat{Z}_2 | \psi(t) \rangle = \pm 1, \quad \langle \psi(t) | (\hat{a}_1 - \hat{a}_2) | \psi(t) \rangle = 0, \quad (23)$$

for  $t \geq \tau$ .

An initial state  $|\psi(0)\rangle$  which is symmetric or anti-symmetric with respect to  $\hat{Z}_2$ , will remain so at all times. If, however, one selects some other initial state without the symmetry prescribed above, then the stochastic evolution will eventually evolve into the block Hilbert subspaces of symmetric or antisymmetric states. This is shown in Fig. 7, where we plot the relative phase  $\phi$  and  $\langle \hat{Z}_2 \rangle$  (dashed line) for two single quantum trajectories (drawn in different colors) which evolve into different subspaces. Here we have considered two values of  $N$  and a low pump value ( $\tilde{F}/\gamma = 0.4$ ).

We can also note that the approach to the symmetric and antisymmetric block subspaces, for the pure state in a quantum trajectory, is delayed with increasing  $N$ . As long as this moment is yet to be attained, the trajectory evidences Josephson-like oscillations. This trend is the precursor of limit cycles as we get close to the  $N \rightarrow \infty$  limit.

In Fig. 8 we show the expectation value of the normalized total number of bosons  $\hat{n}/N$ , the phase difference  $\phi$ , the expectation value of the swapping operator  $\hat{Z}_2$ , and the Fourier transform of  $\phi$ , for a single quantum trajectory and the semiclassical trajectory for different pump values and initial conditions. In the upper panel we consider a pump amplitude far below the bistability region ( $\tilde{F}/\gamma = 0.4$ ) and a normalized initial condition  $|\psi(0)\rangle = |\alpha_1 = 0, \alpha_2 = 0.1\sqrt{N}\rangle$  (in the semiclassical trajectory this corresponds to  $\tilde{\alpha}_1 = 0$  and  $\tilde{\alpha}_2 = 0.1$ ). We can clearly observe that  $\phi$  oscillates with a neat time-crystalline frequency even in the individual quantum trajectories.

In the middle and lower panels of Fig. 8 we show the same as in the upper panel but for an amplitude  $\tilde{F}/\gamma = 1.05$  in the bistability region for two different initial conditions  $|\alpha_1 = 0, \alpha_2 = 0.1\sqrt{N}\rangle$  and  $|\alpha_1 = 0, \alpha_2 = \sqrt{N}\rangle$ , which lead (in the semiclassical evolution) to limit cycles in the lower and upper frequency branches, respectively. In the middle panel we have chosen a quantum trajectory that presents an amplitude switch (from the dark to the bright state) at  $t\gamma \sim 40$  as can be seen in the plot for  $\langle \hat{n} \rangle / N$ . We show in the insets of the middle column that, when the amplitude switch occurs, the frequency of oscillations in  $\phi$  switches between two values (from  $\omega/\gamma \sim 2$  to  $\omega/\gamma \sim 4.7$ ) which correspond to the lower and upper frequency branches of Fig. 5. This means that the known bistability amplitude switching in single quantum trajectories is accompanied, in our model, by a frequency switching. We should mention that this is the general case of complex-amplitude bistability.

The effective decoupling between the bonding and antibonding modes takes place earlier or later in time depending on the value of the nonlinear coefficient  $\tilde{U}$ . A larger value means the two modes are more strongly coupled, thus oscillations decay faster for finite  $N$ . We show this in Fig. 9 for  $\tilde{U}\gamma = 0.5, 1.0$  and  $1.5$ . We can see that for smaller  $\tilde{U}$  the single trajectories take longer times to reach the symmetry subspaces of  $\hat{Z}_2$ , which means that the Josephson-like oscillations live longer. If  $\tilde{U} \rightarrow 0$ , oscillations last forever as the antibonding mode is decoupled from the bonding mode and evolves coherently, as we have explained in the main text as well as here.



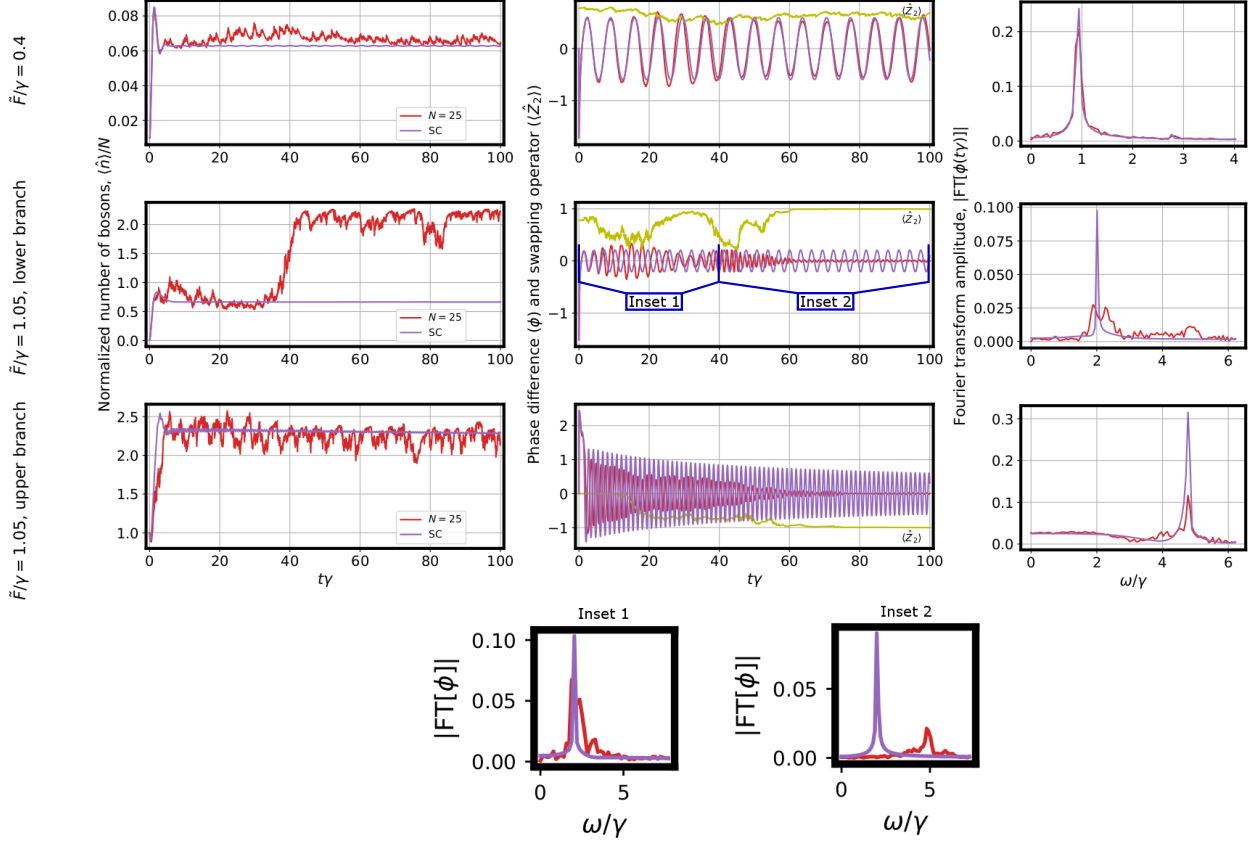


FIG. 8. **Single quantum trajectory and semiclassical trajectory** for two pump values far below (upper panel) and inside (middle and lower panels) the bistability region. The initial states in the upper and middle panels is  $|\psi(0)\rangle = |\alpha_1 = 0, \alpha_2 = 0.1\sqrt{N}\rangle$ , and in the lower panel is  $|\psi(0)\rangle = |\alpha_1 = 0, \alpha_2 = \sqrt{N}\rangle$ . For  $\tilde{F}/\gamma = 1.05$ , these initial states lead respectively to the lower and upper semiclassical branches (both in amplitude and frequency). All the other parameters are the same as in Fig. 2 (and Fig. 1 in the main text).

## MICROSCOPIC DERIVATION OF THE LINDBLAD MASTER EQUATIONS

We consider the system Hamiltonian

$$\begin{aligned} \hat{H} = & \sum_i \omega_c \hat{a}_i^\dagger \hat{a}_i + U \hat{a}_i^\dagger \hat{a}_i^\dagger \hat{a}_i \hat{a}_i - J(\hat{a}_i^\dagger \hat{a}_{i+1} + \hat{a}_i \hat{a}_{i+1}^\dagger) \\ & + F_i(e^{-i\omega_p t} \hat{a}_i^\dagger + e^{i\omega_p t} \hat{a}_i), \end{aligned} \quad (24)$$

in the laboratory frame and a bosonic environment  $\hat{H}_B = \sum_k \omega_k \hat{b}_k^\dagger \hat{b}_k$  initially at thermal equilibrium, described by the density matrix  $\hat{\rho}_B = e^{-\beta \hat{H}_B} / Z_B$ . We assume a linear system-environment coupling, that, in its more general form, can be described by the Hamiltonian

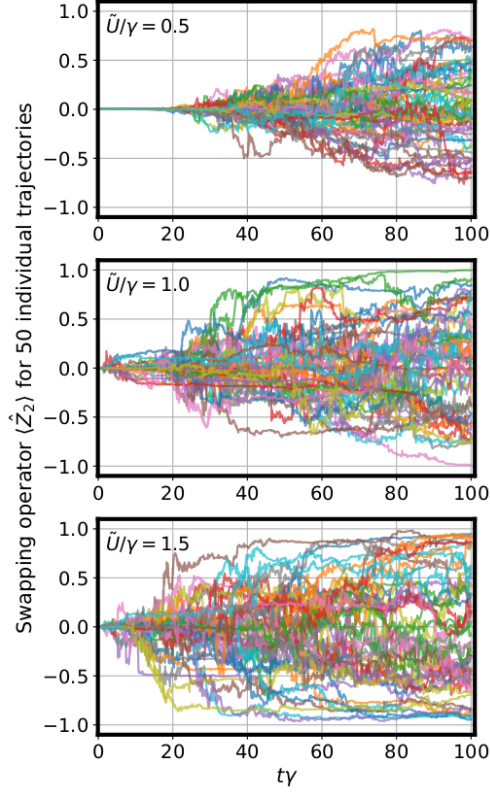


FIG. 9. **Swapping operator expectation value as a function of time for three different values of  $\tilde{U}$**  for 50 individual quantum jump trajectories. For larger  $\tilde{U}$  the trajectories converge faster to the symmetry subspaces of  $\langle \hat{Z}_2 \rangle = \pm 1$ , giving shorter-lived oscillations. The initial state is  $|\psi(0)\rangle = |\alpha_1 = 0, \alpha_2 = \sqrt{N}\rangle$ . The pump amplitude is  $\tilde{F}/\gamma = 0.4$  and  $N = 25$ . All the other parameters are the same as in Fig. 2 (and Fig. 1 in the main text).

$\hat{H}_I = \sum_{k,i} (\gamma_{k,i} \hat{a}_i \hat{b}_k^\dagger + \text{h.c.})$ . Note, however, that by virtue of symmetry, the coefficients  $\gamma_{k,i}$  should be equal for both sites, i.e.,  $\gamma_{k,1} = \gamma_{k,2} \equiv \gamma_k$ . We move to a frame rotating with frequency  $\omega_p$  using the unitary operator

$$\hat{U}_r(t) = \exp \left[ it\omega_p \left( \sum_{i=1,2} \hat{a}_i^\dagger \hat{a}_i + \sum_k \hat{b}_k^\dagger \hat{b}_k \right) \right]. \quad (25)$$

This operation transforms the total Hamiltonian  $\hat{H}_{\text{tot}} = \hat{H} + \hat{H}_B + \hat{H}_I$  into  $\hat{\mathcal{H}}_{\text{tot}} = \hat{\mathcal{H}} + \hat{\mathcal{H}}_B + \hat{\mathcal{H}}_I$ , where

$$\begin{aligned} \hat{\mathcal{H}}_B &= \sum_k (\omega_k - \omega_p) \hat{b}_k^\dagger \hat{b}_k, \\ \hat{\mathcal{H}}_I &= \hat{H}_I = \sum_k \gamma_k (\hat{a}_1 + \hat{a}_2) \hat{b}_k^\dagger + \text{h.c.}, \end{aligned} \quad (26)$$

and  $\hat{\mathcal{H}}$  is given in Eq. (2) in the main text.

As a second step we perform the Born-Markov approximations in the interaction picture. Defining the operator  $\hat{a} \equiv \hat{a}_1 + \hat{a}_2$  for simplicity, one obtains [16]

$$\begin{aligned}
\partial_t \tilde{\rho}(t) &= - \int_0^\infty ds \text{Tr}_B[\tilde{\mathcal{H}}_I(t), [\tilde{\mathcal{H}}_I(t-s), \tilde{\rho}(t) \otimes \hat{\rho}_B]] \\
&= \int_0^\infty ds \left\{ C_1(s) [\tilde{a}^\dagger(t-s) \tilde{\rho}(t) \tilde{a}(t) - \tilde{a}(t) \tilde{a}^\dagger(t-s) \tilde{\rho}(t)] \right. \\
&\quad \left. + C_2(s) [\tilde{a}(t) \tilde{\rho}(t) \tilde{a}^\dagger(t-s) - \tilde{\rho}(t) \tilde{a}^\dagger(t-s) \tilde{a}(t)] \right\} \\
&\quad + \text{h.c.},
\end{aligned} \tag{27}$$

where  $\tilde{O}(t) = e^{it(\hat{\mathcal{H}} + \hat{\mathcal{H}}_B)} \hat{O}(t) e^{-it(\hat{\mathcal{H}} + \hat{\mathcal{H}}_B)}$  is the time evolution of the operator  $\hat{O}(t)$  in the interaction picture. The environment correlation functions read

$$\begin{aligned}
C_1(s) &= \sum_k |\gamma_k|^2 \text{Tr}_B[\tilde{b}_k^\dagger(s) \tilde{b}_k(0) \hat{\rho}_B] \\
&= \sum_k |\gamma_k|^2 e^{is(\omega_k - \omega_p)} n_B(\omega_k), \\
C_2(s) &= \sum_k |\gamma_k|^2 \text{Tr}_B[\tilde{b}_k(0) \tilde{b}_k^\dagger(s) \hat{\rho}_B] \\
&= \sum_k |\gamma_k|^2 e^{is(\omega_k - \omega_p)} [1 + n_B(\omega_k)],
\end{aligned} \tag{28}$$

with  $n_B(x) = (e^{\beta x} - 1)^{-1}$  the Bose-Einstein distribution.

We now make a third approximation that is an alternative to the standard rotating wave (secular) approximation [17]. The environment correlation functions decay on a small time scale  $\tau_B$ , which is the assumption underlying the Markovian approximation. We require that for shorter times ( $s \leq \tau_B$ ) the condition  $\tilde{a}^\dagger(t-s) \simeq \tilde{a}^\dagger(t)$  is satisfied, so that we can integrate only the environment correlation functions. This is only possible if the environment correlation time is much smaller than the smallest time scale of our system, which is, roughly,  $\tau_B \times \max\{|\Delta|, U, -J, F_i\} \ll 1$ . With this condition in hand, and assuming that the environment has a vanishing thermal occupation, we obtain in the Schrödinger picture the Lindblad master equation for nonlocal dissipation Eq. (1) in the main text, with a decay rate  $\gamma = 2\pi\mathcal{S}(\omega_p)$  where

$$\mathcal{S}(\omega) = \sum_k |\gamma_k|^2 \delta(\omega - \omega_k) \tag{29}$$

is the environment spectral density. We have ignored the Lamb-Shift  $\hat{\mathcal{H}}_{LS} = \Omega(\omega_p)(\hat{a}_1^\dagger \hat{a}_1 + \hat{a}_2^\dagger \hat{a}_2)$ , with  $\Omega(\omega_p) = \mathcal{P} \int_0^\infty d\omega \mathcal{S}(\omega)/(\omega_p - \omega)$ , as it can be absorbed by the on-site detuning energy  $\Delta$  of the Hamiltonian. Here,  $\mathcal{P}$  stands for the *principal value*.

The third approximation we have made above can be expressed as  $C_2(s) \simeq C_2(s)e^{\pm i\sigma s} \forall s$ , with  $\sigma \equiv \max\{|\Delta|, U, -J, F_i\}$ . Noting that  $C_2(s) = \int_{-\infty}^\infty d\omega \mathcal{S}(\omega)e^{i(\omega - \omega_p)s}$ , this is fulfilled as long as the spectral density does not vary appreciably around  $\omega_p$  in an interval of width  $2\sigma$  [17]:

$$|\mathcal{S}(\omega_p \pm \sigma) - \mathcal{S}(\omega_p)| \ll \mathcal{S}(\omega_p). \quad (30)$$

This condition is satisfied for Ohmic spectral densities as long as  $\omega_p \gg \sigma$ .

Strictly speaking, because our system has an unbounded Hamiltonian, the condition  $\tau\sigma \ll 1$  may not be enough to safely carry out this approximation. To be more careful, let us proceed to the following definition:

$$\Omega := \{\omega = \epsilon_j - \epsilon_i | \langle \epsilon_i | \hat{\rho}(t) | \epsilon_j \rangle \approx 0 \forall t\}, \quad (31)$$

where  $\{|\epsilon_i\rangle, \epsilon_i\}$  are the eigenkets and eigenenergies of the Hamiltonian  $\hat{\mathcal{H}}$ . If  $\bar{\omega} = \max\{|\bar{\Omega}|\}$ , where  $\bar{\Omega} = \{\text{all frequencies in the system}\}/\Omega$ , then, our condition should read

$$s\bar{\omega} \ll 1 \quad \text{for } s \lesssim \tau_B. \quad (32)$$

This maximum frequency  $\bar{\omega}$  is the highest transition frequency occurring in the dynamic evolution of our system, or, equivalently, the inverse of the smallest time scale characterizing the system response.

Two comments are in order here. The first is that for the derivation of LME with local dissipation, the same procedure outlined here can be used, but one must consider two identical environments, say  $\mathcal{B}_1$  and  $\mathcal{B}_2$ , independently coupled to system modes 1 and 2, respectively. The Hamiltonian operators describing the environments would now read  $\hat{H}_{B_1} = \sum \omega_k \hat{b}_{k,1}^\dagger \hat{b}_{k,1}$  and  $\hat{H}_{B_2} = \sum \omega_k \hat{b}_{k,2}^\dagger \hat{b}_{k,2}$ , where  $\hat{b}_{k,1}$  and  $\hat{b}_{k,2}$  are bosonic operators acting on different environment Fock spaces, i.e.,  $[\hat{b}_{j,1}, \hat{b}_{k,2}] = [\hat{b}_{j,1}, \hat{b}_{k,2}^\dagger] = 0$ , while the system-environment couplings should read  $\hat{H}_{I_1} = \sum_k (\gamma_k \hat{a}_1 \hat{b}_{k,1}^\dagger + \text{h.c.})$  and  $\hat{H}_{I_2} = \sum_k (\gamma_k \hat{a}_2 \hat{b}_{k,2}^\dagger + \text{h.c.})$ , respectively. This is, to the best of our knowledge, the only possible way to derive LME for local dissipation with bosonic baths and linear system-bath couplings. The alternative input-output formalism, or the equivalent collisional models [18], make use of two identical reservoirs alongside the stringent constraint of a constant spectral density.

The second comment concerns the third approximation we used to derive the Lindblad equation. This approximation breaks down in the thermodynamic limit we have considered, for which the energy scales with a parameter  $N$  approaching infinity. This implies that there are time scales in our system smaller than the decay times of bath correlations. We can still, however, probe the system response when one approaches that limit while still remaining under the regime where the approximation is valid. Outside this regime, instead of the third approximation outlined above, one should use the rotating wave (secular) approximation, where fast oscillatory terms are neglected and the system relaxes to thermal equilibrium.

### Imperfections in the symmetric coupling

As we concluded in the main text, the primary difficulty in implementing the configuration of nonlocal dissipation lies on the fact that the two modes of the system may couple with the same strength to the single environment, yet the complex phases of the coupling constants,  $\gamma_{k,i}$ , may differ between  $i = 1, 2$ . In the following we briefly discuss this possibility.

Let us write the coupling constants in the form  $\gamma_{k,i} = \gamma_k e^{i\phi_{k,i}}$ , defining the difference between the two phases as  $\Delta\phi_k \equiv \phi_{k,1} - \phi_{k,2}$ . In this case, the LME in the Schrödinger picture reads

$$\partial_t \hat{\rho} = -i \left[ \hat{\mathcal{H}} + \sum_{ij} \Omega_{ij}(\omega_p) \hat{a}_j^\dagger \hat{a}_i, \hat{\rho} \right] + 2\pi \sum_{ij} S_{ij}(\omega_p) \left( \hat{a}_i \hat{\rho} \hat{a}_j^\dagger - \frac{1}{2} \{ \hat{a}_j^\dagger \hat{a}_i, \hat{\rho} \} \right), \quad (33)$$

with  $\Omega_{ij}(\omega_p) = -\mathcal{P} \int_0^\infty d\omega \frac{S_{ij}(\omega)}{\omega - \omega_p}$ , and  $S_{ij}(\omega) = \sum_k |\gamma_k|^2 e^{i(\phi_{k,i} - \phi_{k,j})} \delta(\omega_k - \omega)$ . We note that the first-order (in  $\Delta\phi_k$ ) contribution to the Lamb-Shift vanishes; therefore, only the zero-order term remains which can be absorbed into the detuning  $\Delta$ , which is what we have done before. In order to recast the dissipation in diagonal form, we can define a new operator

$$\hat{c}_k = \frac{1}{\sqrt{2}} (e^{i\Delta\phi_k/2} \hat{a}_1 + e^{-i\Delta\phi_k/2} \hat{a}_2) = \cos(\Delta\phi_k/2) \hat{a}_B + i \sin(\Delta\phi_k/2) \hat{a}_A, \quad (34)$$

obtaining the corresponding dissipator

$$\mathcal{D}(\hat{\rho}) = 4\pi \sum_k |\gamma_k|^2 \delta(\omega_k - \omega_p) \left( \hat{c}_k \hat{\rho} \hat{c}_k^\dagger - \frac{1}{2} \{ \hat{c}_k^\dagger \hat{c}_k, \hat{\rho} \} \right). \quad (35)$$

The new Lindblad operator in Eq. (35) does not commute with  $\hat{Z}_2$ , hence it breaks explicitly the continuous swapping symmetry. Due to the presence of the Dirac delta-function, however, the only relevant  $k$ -modes are those near the pump frequency  $\omega_p$ . This

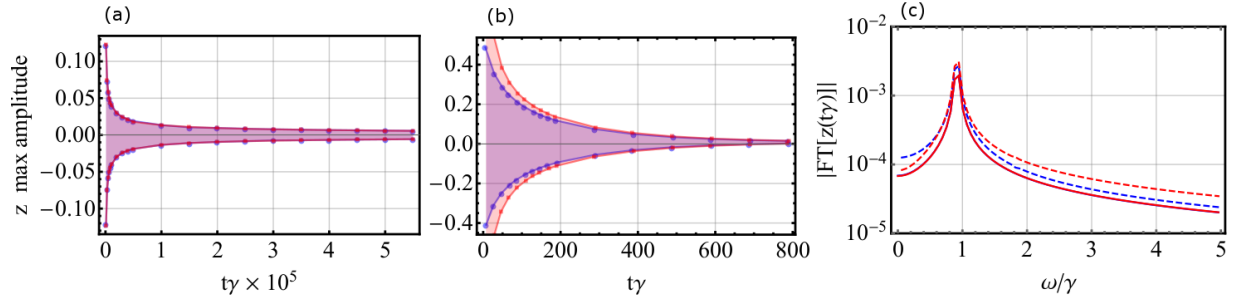


FIG. 10. **Long-lived oscillations for perfect and imperfect nonlocal dissipation.** Frames (a) and (b) show the envelope of the oscillating population difference  $z = |\tilde{\alpha}_1|^2 - |\tilde{\alpha}_2|^2$  for perfect and imperfect nonlocal dissipation, respectively. Two random initial conditions were chosen, and are depicted in different colors. Frame (c) shows a Fourier transformation of  $z$  in a time window of  $100\gamma^{-1}$  at the end of the evolution shown in (a) and (b). Continuous (dashed) lines correspond to perfect (imperfect) dissipation. The pump is  $\tilde{F}/\gamma = 0.4$ , and all the other parameters are same as in Fig. 1 in the main text.

means that in order for the dissipation to break the symmetry there must be a nonnegligible phase difference  $\Delta\phi_k$  for  $\omega_k \approx \omega_p$ . If that difference is small yet finite, the main contribution to the dissipation will be due to the bonding mode  $\hat{a}_B$ , as  $\hat{c}_k \approx \hat{a}_B + i(\Delta\phi_k/2)\hat{a}_A$ . Such a dissipator lifts the zero-eigenvalue degeneracy of the Liouvillian, and, as we have numerically verified, destroys also the semiclassical limit cycles. Long-lived oscillations can still be observed if  $\Delta\phi_k$  is small enough. To illustrate this point, we study the long-time dynamics of the semiclassical equations of motion obtained from the new evolution  $\partial_t \hat{\rho} = -i[\hat{\mathcal{H}}, \hat{\rho}] + 2\gamma\mathcal{D}[\hat{c}_p](\hat{\rho})$ , where  $\gamma = 2\pi \sum_k |\gamma_k|^2 \delta(\omega_k - \omega_p)$  and  $\hat{c}_p$  is given by Eq. (34) for the mode  $\omega_p$ . The modified (rescaled) Gross-Pitaevskii equations read

$$\begin{aligned} i\partial_t \tilde{\alpha}_1 &= (-\Delta - i\gamma/2 + 2\tilde{U}|\tilde{\alpha}_1|^2)\tilde{\alpha}_1 - (J + ie^{-i\Delta\phi_p}\gamma/2)\tilde{\alpha}_2 + \tilde{F}, \\ i\partial_t \tilde{\alpha}_2 &= (-\Delta - i\gamma/2 + 2\tilde{U}|\tilde{\alpha}_2|^2)\tilde{\alpha}_2 - (J + ie^{i\Delta\phi_p}\gamma/2)\tilde{\alpha}_1 + \tilde{F}. \end{aligned} \quad (36)$$

The new terms  $e^{\pm i\Delta\phi_p}$  introduced have real and imaginary parts. The imaginary part will be added to the coherent part of the dynamics and is relatively innocuous. What is really important is the real part, which adds a local dissipation contribution to the system. We choose  $\Delta\phi_p = \cos^{-1}(0.99)$  to yield 1% (99%) of local (nonlocal) dissipation, and compare in the long time-behaviour, as predicted in Eqs. (18) and (36) and depicted in Fig. 10. In Fig. 10(a) and (b) we show the envelope of the oscillating population difference  $z(\tau) =$

$|\tilde{\alpha}_1(\tau)|^2 - |\tilde{\alpha}_2(\tau)|^2$  for perfect and imperfect nonlocal dissipation, respectively. In each case we have chosen two random initial conditions, shown in different colors. For perfect nonlocal dissipation,  $z$  slowly converge to its final oscillatory form at very large times ( $t\gamma \sim 3.5 \times 10^5$ ), while for imperfect dissipation,  $z$  goes to zero and the relaxation is much faster ( $t\gamma \sim 800$ ); it is, however, very slow compared to the time scale set by decay rate  $\gamma$ , which means that the oscillatory behaviour could be observed in the laboratory even in the presence of imperfect nonlocal dissipation.

Another important aspect characterizing the inclusion of the perturbative terms is the period robustness. In Fig. 10(c) we show a Fourier transformation of  $z$  in a time window of  $100\gamma^{-1}$  at the end of the evolution shown in Fig. 10(a) and (b). In blue and red lines (dashed lines) we show the Fourier transformation for perfect (imperfect) nonlocal dissipation. We can see that the frequency peak ( $\omega/\gamma \approx 0.9424$ ) is the same in both cases, independently of the initial condition. A similar frequency robustness over driving imperfections has been experimentally observed in a *Discrete Time Crystal* [19].

---

\* electronic address: c.lledo.17@ucl.ac.uk

- [1] Victor V. Albert and Liang Jiang, “Symmetries and conserved quantities in lindblad master equations,” *Phys. Rev. A* **89**, 022118 (2014).
- [2] Davide Nigro, “On the uniqueness of the steady-state solution of the lindblad–gorini–kossakowski–sudarshan equation,” *J. Stat. Mech.* **2019**, 043202 (2019).
- [3] Bin Cao, Khan W. Mahmud, and Mohammad Hafezi, “Two coupled nonlinear cavities in a driven-dissipative environment,” *Phys. Rev. A* **94**, 063805 (2016).
- [4] Wim Casteels and Cristiano Ciuti, “Quantum entanglement in the spatial-symmetry-breaking phase transition of a driven-dissipative bose-hubbard dimer,” *Phys. Rev. A* **95**, 013812 (2017).
- [5] A time crystal has a limit cycle in the  $N \rightarrow \infty$  limit, spontaneously breaking the time-translation symmetry. See: F. Iemini, A. Russomanno, J. Keeling, M. Schirò, M. Dalmonte, and R. Fazio, “Boundary time crystals,” *Phys. Rev. Lett.* **121**, 035301 (2018); Zongping Gong, Ryusuke Hamazaki, and Masahito Ueda, “Discrete time-crystalline order in cavity and circuit qed systems,” *Phys. Rev. Lett.* **120**, 040404 (2018); Reuben R. W. Wang, Bo Xing, Gabriel G. Carlo, and Dario Poletti, “Period doubling in period-one steady states,” *Phys.*

- Rev. E **97**, 020202(R) (2018).
- [6] Berislav Buca, Joseph Tindall, and Dieter Jaksch, “Non-stationary coherent quantum many-body dynamics through dissipation,” *Nat. Commun.* **10** (2019).
  - [7] Wim Casteels and Michiel Wouters, “Optically bistable driven-dissipative bose-hubbard dimer: Gutzwiller approaches and entanglement,” *Phys. Rev. A* **95**, 043833 (2017).
  - [8] E. M. Kessler, G. Giedke, A. Imamoglu, S. F. Yelin, M. D. Lukin, and J. I. Cirac, “Dissipative phase transition in a central spin system,” *Phys. Rev. A* **86**, 012116 (2012).
  - [9] Fabrizio Minganti, Alberto Biella, Nicola Bartolo, and Cristiano Ciuti, “Spectral theory of liouvillians for dissipative phase transitions,” *Phys. Rev. A* **98**, 042118 (2018).
  - [10] Thomas Fink, Anne Schade, Sven Höfling, Christian Schneider, and Ataç Imamoglu, “Signatures of a dissipative phase transition in photon correlation measurements,” *Nat. Phys.* **14**, 365–369 (2018).
  - [11] I. L. Aleiner, B. L. Altshuler, and Y. G. Rubo, “Radiative coupling and weak lasing of exciton-polariton condensates,” *Phys. Rev. B* **85**, 121301(R) (2012).
  - [12] K. Rayanov, B. L. Altshuler, Y. G. Rubo, and S. Flach, “Frequency combs with weakly lasing exciton-polariton condensates,” *Phys. Rev. Lett.* **114**, 193901 (2015).
  - [13] S. R. K. Rodriguez, W. Casteels, F. Storme, N. Carlon Zambon, I. Sagnes, L. Le Gratiet, E. Galopin, A. Lemaître, A. Amo, C. Ciuti, and J. Bloch, “Probing a dissipative phase transition via dynamical optical hysteresis,” *Phys. Rev. Lett.* **118**, 247402 (2017).
  - [14] Katarzyna Macieszczak, M. Guță, Igor Lesanovsky, and Juan P. Garrahan, “Towards a theory of metastability in open quantum dynamics,” *Phys. Rev. Lett.* **116**, 240404 (2016).
  - [15] M. B. Plenio and P. L. Knight, “The quantum-jump approach to dissipative dynamics in quantum optics,” *Rev. Mod. Phys.* **70**, 101–144 (1998).
  - [16] H.-P. Breuer and F. Petruccione, *The Theory of Open Quantum Systems* (Oxford University Press, New York, 2002).
  - [17] Patrick P Hofer, Mart Perarnau-Llobet, L David M Miranda, Graldine Haack, Ralph Silva, Jonatan Bohr Brask, and Nicolas Brunner, “Markovian master equations for quantum thermal machines: local versus global approach,” *New J. Phys.* **19**, 123037 (2017).
  - [18] Francesco Ciccarello, “Collision models in quantum optics,” *Quantum Meas. Quantum Metrol.* **4**, 53–63 (2018).
  - [19] Soonwon Choi, Joonhee Choi, Renate Landig, Georg Kucsko, Hengyun Zhou, Junichi Isoya,



Fedor Jelezko, Shinobu Onoda, Hitoshi Sumiya, Vedika Khemani, Curt Von Keyserlingk, Norman Y. Yao, Eugene Demler, and Mikhail D. Lukin, “Observation of discrete time-crystalline order in a disordered dipolar many-body system,” *Nature (London)* **543**, 221–225 (2017).